Human Molecular Genetics, 2012, Vol. 21, No. 20 **4378–4393**
doi:10.1093/hmg/dds271
Advance Access published on July 13, 2012

Dystrophin and utrophin expression require sarcospan: loss of α7 integrin exacerbates a newly discovered muscle phenotype in sarcospan-null mice

Jamie L. Marshall[1], Eric Chou[1], Jennifer Oh[1], Allan Kwok[1], Dean J. Burkin[2] and Rachelle H. Crosbie-Watson[1,3,*]

[1]Department of Integrative Biology and Physiology, University of California, Los Angeles, CA 90095, USA, [2]Department of Pharmacology, Center for Molecular Medicine, University of Nevada School of Medicine, Reno, NV 89557, USA and [3]Molecular Biology Institute, University of California, Los Angeles, CA 90095, USA

Received April 18, 2012; Revised June 14, 2012; Accepted July 6, 2012

Sarcospan (SSPN) is a core component of the major adhesion complexes in skeletal muscle, the dystrophin– and utrophin (Utr)–glycoprotein complexes (DGC and UGC). We performed a rigorous analysis of SSPN-null mice and discovered that loss of SSPN decreased DGC and UGC abundance, leading to impaired laminin-binding activity and susceptibility to eccentric contraction-induced injury in skeletal muscle. We show that loss of SSPN increased levels of α7β1 integrin. To genetically test whether integrin compensates for the loss of DGC and UGC function in SSPN-nulls, we generated mice lacking both SSPN and α7 integrin (DKO, double knockout). Muscle regeneration, sarcolemma integrity and fibrosis were exacerbated in DKO mice and were remarkably similar to muscle from Duchenne muscular dystrophy (DMD) patients, suggesting that secondary loss of integrin contributes significantly to pathogenesis. Expression of the DGC and UGC, laminin binding and Akt signaling were negatively impacted in DKO muscle, resulting in severely diminished specific force properties. We demonstrate that SSPN is a necessary component of dystrophin and Utr function and that SSPN modulation of integrin signaling is required for extracellular matrix attachment and muscle force development.

INTRODUCTION

Three adhesion glycoprotein complexes span the sarcolemma and protect muscle from contraction-induced damage by maintaining connections between filamentous actin and the extracellular matrix (ECM): the dystrophin–glycoprotein complex (DGC), the utrophin (Utr)–glycoprotein complex (UGC) and the α7β1 integrin complex (1,2). Dystrophin, located at the subsarcolemma, is a component of the DGC that interacts with filamentous actin and β-dystroglycan (β-DG) (3). α-DG binds to ligands in the ECM through a heavily glycosylated mucin domain and is anchored to the sarcolemma via β-DG (4,5). The sarcoglycan–SSPN (SG-SSPN) subcomplex consists of four transmembrane glycoproteins referred to as the SGs (α-, β-, γ- and δ-SG) and SSPN. The UGC is homologous to the DGC except that Utr replaces dystrophin. The localization of the UGC is restricted to neuromuscular (NMJ) and myotendinous (MTJ) junctions in normal adult muscle (6–8). Similar to the DGC, the α7β1 integrin complex is localized to the extra-synaptic sarcolemma, is enriched at NMJs and MTJs and is also a laminin α2 receptor (9–13). Direct physical interactions between α7β1 integrin and the UGC or DGC have never been demonstrated in adult skeletal muscle.

Mutations in most of the components of the three-glycoprotein adhesion complexes result in various forms of muscular dystrophy. The concept of compensatory glycoprotein

*To whom correspondence should be addressed at: Department of Integrative Biology and Physiology, University of California Los Angeles, 610 Charles E. Young Drive East, Terasaki Life Sciences Building, Room 1121, Los Angeles, CA 90095, USA. Tel: +1 3107942103; Fax: +1 3102063987; Email: rcrosbie@physci.ucla.edu

adhesion complexes arose from genetic studies utilizing dystrophin-deficient *mdx* mice, which serve as a model for DMD (14). Initial observations that *mdx* mice demonstrate an attenuated form of muscular dystrophy and maintain normal lifespan compared with DMD boys led to the hypothesis that the increased levels of UGC and α7β1 integrin perform redundant functions, thus compensating for the absence of DGC (6–8,15–19). Evidence to support this hypothesis is derived from studies in which additional genetic removal of either Utr or α7 integrin (Itgα7) from *mdx* mice increased the severity of dystrophic pathology and greatly reduced the lifespan (20–23). Furthermore, over-expression of either Utr or β1 integrin in *mdx* mice and that of Itgα7 in *mdx*: Utr-null mice ameliorate dystrophic pathology (24–29), supporting the concept of functional redundancy of the DGC, UGC and α7β1 integrin complexes in murine skeletal muscle.

SSPN is a core component of the DGC and UGC, and its tetraspanin-like properties suggest that it may affect integrin expression (30,31). Thus, SSPN has the potential to regulate cross-talk between all three adhesion glycoprotein complexes. Although young SSPN-deficient mice display a normal muscle phenotype without force deficits (32), we now show that loss of SSPN in aged mice increases α7β1 integrin expression. In the current report, we crossed SSPN-deficient mice with Itgα7-deficient mice to create double-knockout (DKO) mice. Itgα7-deficient mice suffer from a late onset myopathy (33), decrease in force transmission in the diaphragm of 5-month-old mice (34) and altered development of NMJs (35,36) and MTJs (33,37). We test the hypothesis that increased Itgα7 levels in SSPN-null mice compensate for SSPN deficiency.

RESULTS

Levels of α7β1 integrin are increased in SSPN-deficient mice

In DMD patients and *mdx* mice, increased expression of α7β1 integrin and the UGC at the extra-synaptic sarcolemma compensates for the loss of the DGC (6,7,16,19,38–41). To first investigate whether these proteins functioned in a compensatory fashion in SSPN-deficient mice, we analyzed total skeletal muscle protein lysates from adult 4.5-month-old wild-type and SSPN-null mice. Utr, DGs (α- and β-DGs), SGs (α- and γ-SGs), phosphorylated Akt (Serine 473 and Threonine 308), phosphorylated p70S6K, matrix metalloproteinase 9 (MMP 9), phosphorylated mitogen-activated protein kinase (MAPK) p44 and phosphorylated nuclear factor-κB1 (NF-κB1) p105 are reduced in SSPN-deficient muscle relative to wild-type controls (Fig. 1). Quantification of the representative blots in Figure 1 revealed that the reductions observed in the activation of Akt and downstream p70S6K are significant in SSPN-deficient muscle compared with wild-type (Supplementary Material, Fig. S1). Interestingly, we observed an increase in β1D integrin and the activation of p38 MAPK (p-p38) levels in SSPN-null muscle (Fig. 1), raising the possibility that integrin expression compensates for the loss of SSPN function, thereby masking any SSPN-related phenotypes.

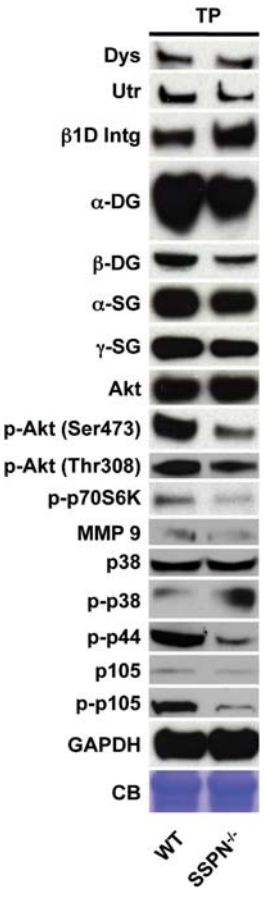

Figure 1. Integrin is increased in SSPN-deficient muscle. Skeletal muscle lysates from 4.5-month-old wild-type (WT) and SSPN-null ($SSPN^{-/-}$) mice were prepared in modified RIPA buffer. Equal protein samples (60 μg) were resolved by SDS–PAGE. Immunoblotting was performed with antibodies against dystrophin (Dys), utrophin (Utr), β1D integrin (β1D Intg), DGs (α- and β-DG), SGs (α- and γ-SG), Akt, phosphorylated Akt (p-Akt, Ser473), phosphorylated Akt (p-Akt, Thr308), phosphorylated p70S6K (p-p70S6K), matrix metalloproteinase 9 (MMP 9), p38 MAPK (p38), phosphorylated p38 MAPK (p-p38), phosphorylated p44 MAPK (p-p44), NF-κB1 p105 (p105), phosphorylated NF-κB1 p105 (p-p105). GAPDH and Coomassie blue (CB) staining serve as loading controls. Quantification of p-Akt/Akt, p-p70S6K and p-IGF-R/IGF-R are provided in Supplementary Material, Figure S1.

Genetic removal of SSPN from Itgα7-null mice exacerbates muscle atrophy and causes premature lethality

To determine whether increased integrin levels compensate for the loss of SSPN, we crossed Itgα7-null females with SSPN-deficient males to generate mice lacking both Itgα7 and SSPN (DKO). Itgα7-deficient mice exhibit reduced grip strength and a late onset, mild myopathy at ∼4 months of age (33,42). As an initial test for the effect of SSPN on integrin function, we investigated whether loss of SSPN affects myopathy in aged Itgα7-deficient mice. We first analyzed body size and skeletal structure by macroscopic evaluation of 4.5- and 6-month-old mice, generated a survival curve and collected data on genotype frequencies. DKO mice demonstrate significant reductions in body weight and wet muscle mass compared with wild-type and SSPN-deficient controls (Supplementary Material, Fig. S2A–F). At 4.5 months,

Itgα7-deficient mice exhibit mild kyphosis relative to SSPN-null and wild-type controls (Fig. 2A). By comparison, DKO mice display severe kyphosis at 4.5 months as evidenced by the steep slope of the spine behind the shoulder blades, which is exacerbated at 6 months of age (Fig. 2A and B). Kyphosis results from weakening of the muscles supporting the back (43), demonstrating that the removal of SSPN from Itgα7-deficient mice increases the severity of skeletal muscle atrophy. As depicted in the Kaplan–Meier survival analysis, 10% of DKO mice do not survive past 4 weeks of age compared with 5% of Itgα7-deficient controls (Fig. 2C). DKO mice failed to thrive throughout the experimental time frame, as evidenced by the significantly reduced viability (50%) of DKO mice at 8 months (Fig. 2C). We observed 3-fold more live DKO births compared with Itgα7-deficient controls (Table 1), suggesting that additional removal of SSPN paradoxically ameliorates embryonic lethality in Itgα7-deficient controls.

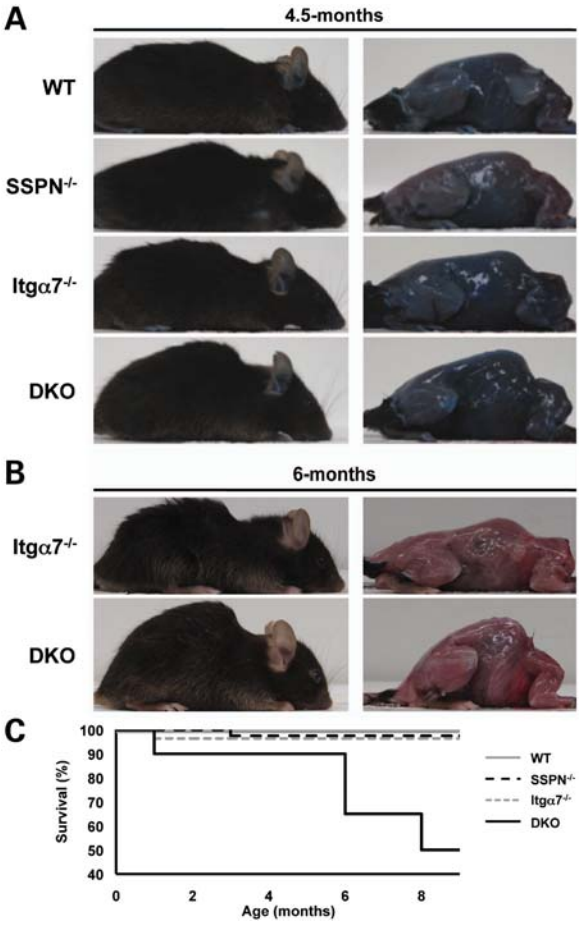

Figure 2. Severe kyphosis in SSPN- and α7 integrin-deficient (DKO) mice. (**A**) Photographs of wild-type (WT), SSPN-null ($SSPN^{-/-}$), α7 integrin-null ($Itg\alpha7^{-/-}$) and SSPN-null:α7 integrin-null (DKO) mice at 4.5 months of age (left panels). Macroscopic evaluation of musculoskeletal structure in mice that were injected with EBD (right panels). DKO mice display severe kyphosis compared with control littermates. (**B**) Photographs of α7 integrin-null ($Itg\alpha7^{-/-}$) and SSPN-null:α7 integrin-null (DKO) mice at 6 months of age. DKO mice continue to exhibit severe kyphosis compared with control littermates. (**C**) The viability of DKO ($n = 20$) mice is severely reduced between 6 and 9 months of age compared with wild-type ($n = 20$), α7 integrin-null ($n = 20$) and SSPN-null ($n = 20$) mice. At 8 months, only 50% of DKO mice remain viable.

DKO mice exhibit muscle pathology

Many forms of muscular dystrophy are characterized by detachment of the sarcolemma from either the ECM and/or the intracellular filamentous actin cytoskeleton, leading to cycles of myofiber degeneration and regeneration, satellite cell exhaustion and replacement of muscle with fibrotic tissue and fat (44). To evaluate whether loss of SSPN affects the Itgα7-deficient phenotype, quadriceps and diaphragm muscles were analyzed for muscle regeneration, degeneration, fibrosis deposition and adipose replacement. At 4.5 months of age, Itgα7-deficient mice displayed mild myopathy evidenced by necrosis and centrally placed nuclei in hematoxylin and eosin (H&E)-stained transverse cryosections of quadriceps muscle (Fig. 3A). Pathological symptoms remained absent in SSPN-deficient and Itgα7-deficient muscle at these older ages. Central nucleation, a marker for muscle regeneration, was significantly increased in DKO mice at 4.5 months of age compared with all controls, demonstrating that loss of SSPN and Itgα7 exacerbates myofiber regeneration (Fig. 3A and B).

Sarcolemmal instability is one of the hallmark symptoms of dystrophic pathology. Using an Evan's blue dye (EBD) tracer assay, we investigated the possibility that the combined loss of both SSPN and Itgα7 caused sarcolemma damage. EBD is a fluorescent dye that is administered via an intraperitoneal route and accumulates in the interior of damaged muscle fibers, where it is detected using fluorescence microscopy (45). Transverse quadriceps muscle sections collected from EBD-treated mice were stained with laminin antibodies (green) as a sarcolemmal marker (Fig. 3A). We demonstrate that EBD accumulation (red) is statistically increased in DKO quadriceps muscle at 4.5 months of age relative to controls (Fig. 3C), whereas the individual loss of either SSPN or Itgα7 was insufficient to cause membrane damage. It is particularly noteworthy that laminin levels are severely diminished in DKO samples (Fig. 3A).

Macroscopic evaluation demonstrated significant differences in myofiber size in DKO mice relative to all controls (Fig. 3A). Quantification of transverse cross-sectional areas (CSAs) of quadriceps muscles revealed that SSPN-deficient and Itgα7-deficient mice exhibit a rightward shift (larger CSAs) in the myofiber distribution profile compared with wild-type controls. These single knockouts exhibit a larger proportion of myofibers ranging between 2500 and 5000 μm^2 and a corresponding reduction of myofibers with CSAs $<2500\ \mu m^2$ (Fig. 3D). Conversely, DKO muscle displays a leftward shift (smaller CSA) in the distribution profile as revealed by the increased percentage of fibers with CSAs between 0 and 2000 μm^2 and a corresponding decrease in fibers $>2000\ \mu m^2$ (Fig. 3D). We provide evidence that the combined loss of Itgα7 and SSPN in quadriceps muscles significantly attenuates the median myofiber CSA, resulting in greater numbers of smaller myofibers (Fig. 3E). We discovered that the trends in myofiber CSA correlate with muscle weight. Quadriceps muscle isolated from SSPN-deficient mice weigh significantly more than wild-type controls,

Table 1. Improved embryonic survival in DKO mice compared with α7 integrin-null mice

Genotype	Predicted	Observed
WT	6.3%	21.0% (11/52)
$SSPN^{-/-}$	6.3%	17.0% (9/52)
$Itg\alpha7^{-/-}$	6.3%	4.0% (2/52)
DKO	6.3%	12.0% (6/52)

Predicted and observed genotype probabilities for wild-type (WT), SSPN-null ($SSPN^{-/-}$), α7 integrin-null ($Itg\alpha7^{-/-}$) and SSPN-null:α7 integrin-null (DKO) mice are represented. α7 integrin and SSPN heterozygous mice ($Itg\alpha7^{+/-}$:$SSPN^{+/-}$) were crossed, yielding a 6.25% probability for each genotype in the resultant litters. Genotypes and their relative representation for more than 50 progeny were determined when mice were 1.5 weeks of age. α7 integrin-null mice display increased partial embryonic lethality, which is consistent with previous observations (75). The additional loss of SSPN doubled the expected survival rate of α7 integrin-null mice (DKO), although the survival rate remains less than the numbers observed for wild-type and SSPN-null controls.

whereas DKO quadriceps weigh significantly less than single knockout controls (Supplementary Material, Fig. S2C).

In the *mdx* mouse model of DMD, the diaphragm is the most severely affected muscle, as evidenced by robust fibrosis and fat deposition (46). To further investigate the relationship between SSPN and Itgα7, diaphragm muscles were analyzed for markers of dystrophic pathology at 4.5, 6 and 9 months of age. H&E histological analysis of transverse diaphragm cryosections revealed increased interstitial connective tissue between myofibers in Itgα7-deficient mice, which was more evident in DKO muscle (Fig. 4A). At 4.5 months of age, SSPN-deficient and Itgα7-deficient mice do not display signs of fibrosis; however, DKO mice exhibit a dramatic increase in collagen deposition as revealed by Van Geison staining that was remarkably analogous to DMD muscle. Representative images of H&E-stained whole diaphragms from 4.5-month-old Itgα7-deficient and DKO mice are provided to illustrate widespread fibrosis and adiposity in DKO samples (Supplementary Material, Fig. S3). The Itgα7-deficient mice exhibit detectable collagen deposition at 6 months; however, the myopathy in the DKO mice is more severe than that in the Itgα7 single knockout. Collagen deposition was undetectable in SSPN-deficient mice at all ages examined. At 9 months, the DKO diaphragms display significant fibrotic collagen deposition and fat replacement in the diaphragm (Fig. 4A). Oil Red staining, a marker for adipose cells and lipid deposits, is not detectable in mice at 4.5 months of age. However, Itgα7 single null and DKO mice display Oil Red staining at 6 months, which is exacerbated in the DKOs at 9 months of age (Fig. 4A).

Quantification of central nucleation in the diaphragm (4.5 months) revealed a 16-fold increase in regeneration in DKO mice relative to all controls (Fig. 4B). Embryonic myosin heavy chain (eMHC) staining, which identifies newly regenerated fibers, was detected in DKO diaphragms, suggesting that markers for early stages of regeneration are normally expressed (Supplementary Material, Fig. S4A). SSPN-null and Itgα7-null mice display wild-type levels of regeneration in the diaphragm at this age (Fig. 4B). CSA distribution profiles for single-mutant muscle were similar to wild-type (Fig. 4C and D). DKO diaphragms exhibit greater numbers of small fibers (0–500 μm^2) and fewer large fibers with CSAs greater than 500 μm^2 compared with all controls (Fig. 4C). Similar to the quadriceps muscle, DKO diaphragms display more than a 2-fold increase in the percentage of very small (0–500 μm^2) myofibers (Fig. 4D), consistent with the observed increases in collagen deposition and regeneration.

Akt signaling and levels of DGC/UGC are diminished in DKO muscle

Several recent studies have uncovered the important role of intracellular signaling in regulating muscle strength, hypertrophy and pathophysiology. One of the main pathways to govern these physiological events is the stimulation of the phosphatidylinositol-3 kinase/Akt signaling pathway leading to downstream activation of p70S6K protein synthesis pathways (47,48). Activation of the Akt signaling pathway occurs through many different membrane receptors, including insulin-like growth factor 1 (IGF-1), growth and differentiation factor 8 or myostatin and β1 integrin-associated integrin-linked kinase (ILK) (47–49). Loss of Akt signaling in mice results in severe muscle atrophy, fetal growth retardation and neonatal lethality (50). Over-expression of constitutively active Akt in dystrophin-deficient *mdx* mice results in a functional amelioration of the sarcolemma through up-regulation of Utr and α7β1 integrin, which leads to an improvement in force generation (51,52). To determine whether defects observed in the DKO mice involve deficiencies in the Akt pathway, we performed immunoblotting on total skeletal muscle protein lysates to determine relative levels of phosphorylated proteins within the signaling axis. Phosphorylation of Akt, p70S6K and IGF-1 receptor was decreased in DKO muscle, accompanied by an increase in myostatin levels (Fig. 5A; Supplementary Material, Fig. S1A–D). Myostatin has been shown to negatively attenuate the activated Akt/p70S6K pathway, which is associated with skeletal muscle atrophy (47,53). Furthermore, IGF-1 levels decrease with age and are correlated with muscle cachexia. When over-expressed, IGF-1 augments force generation capacity, reduces fibrosis in the diaphragms of aged *mdx* mice and prevents normal loss of muscle mass associated with senescence in 2-year-old wild-type mice (54–56).

In addition to the Akt pathway, MMPs, MAPK signaling and NF-κB1 signaling are important in tissue remodeling and disease progression in several pathophysiological conditions in skeletal muscle. MMP 9 has been shown to be deleteriously increased in the *mdx* mouse model of DMD because inhibition of MMP 9 alleviates dystrophic pathology in young *mdx* mice and reduces myofiber injury in the diaphragm of old *mdx* mice (57–59). In muscle, over-expression of MMP 9 increased the levels of contractile proteins and force production in isometric contractions while reducing the level of collagen deposition in the ECM (57), demonstrating the importance of MMP 9 in remodeling the ECM. Although the role of p38 MAPK in skeletal muscle disease remains unclear, it has been hypothesized that activated p-38 MAPK stimulates the transcriptional activity of NF-κB1 which promotes an increase in an increase in the transcription of MMP 9 (60). NF-κB signaling has been shown to be persistently elevated

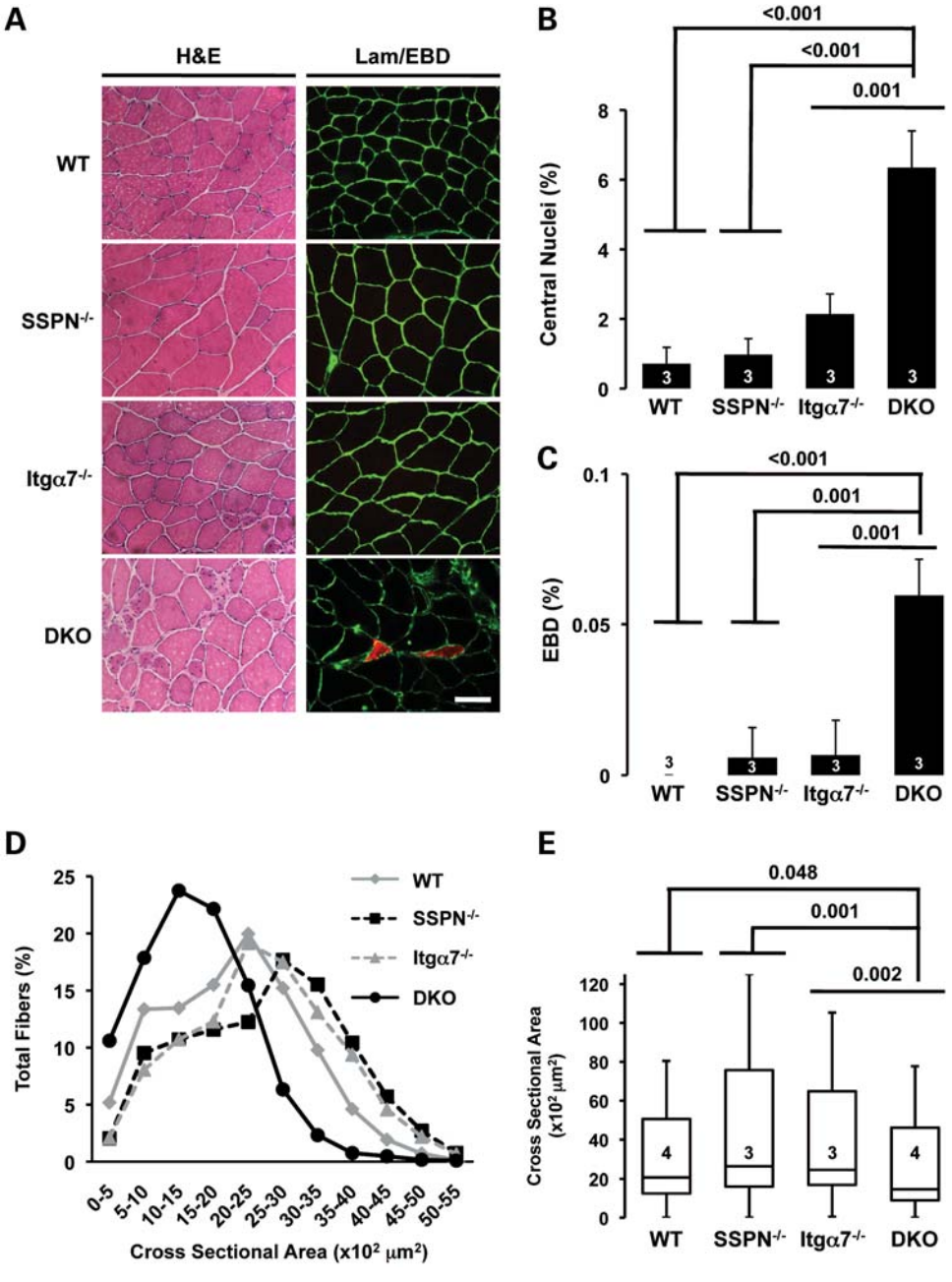

Figure 3. Enhanced muscle pathology in DKO mice compared with α7 integrin-null mice. (**A**) Transverse quadriceps sections from wild-type (WT), SSPN-null ($SSPN^{-/-}$), α7 integrin-null ($Itg\alpha7^{-/-}$) and SSPN-null:α7 integrin-null (DKO) mice were stained for H&E to visualize nuclei and muscle pathology (left panels). Muscle cryosections from EBD-treated mice were incubated with laminin antibodies (green) to delineate the sarcolemma (right panels). EBD-positive fibers were visualized by red fluorescence, which serves as a marker for sarcolemma damage. Bar, 50 μm. (**B**) Muscle regeneration was evaluated by quantification of myofibers with central nuclei. Wild-type, SSPN-null and α7 integrin-null mice had <2% of fibers with centrally placed nuclei. The additional loss of SSPN resulted in a 3-fold increase in central nuclei in mice lacking α7 integrin (DKO). (**C**) Membrane damage was assayed by quantification of EBD uptake into quadriceps muscle fibers. Data are presented as an average and error bars represent standard deviation of the mean. (**D**) Myofiber CSA was quantified on transverse quadriceps cryosections stained with laminin to delineate myofiber boundaries for wild-type (WT) ($n = 4$), SSPN-null ($SSPN^{-/-}$) ($n = 3$), α7 integrin-null ($Itg\alpha7^{-/-}$) ($n = 3$) and SSPN-null:α7 integrin-null (DKO) ($n = 4$) mice. SSPN-null and α7 integrin-null muscle exhibit myofiber hypertrophy compared with wild-type and DKO muscle. Average CSAs are plotted as an average percentage of total fibers (700 myofibers were analyzed per quadriceps). (**E**) Box plots demonstrating the variance and mean muscle fiber CSA of the data shown in (D). Median DKO myofibers are significantly hypotrophic compared with all controls. Boxes represent the middle quartiles from the 25th to 75th percentiles. Error bars represent maximum and minimum CSAs and statistics were calculated comparing the means. For (B)–(E), statistics were calculated using an ANOVA and Bonferroni's correction or Tukey's test. *n*- and *P*-values are indicated on the plots.

in the immune infiltrate and regenerating myofibers of DMD patients and *mdx* mice. Specifically, NF-κB signaling functions to inhibit muscle progenitor cells and to promote inflammation and myofiber necrosis in activated macrophages (61). Preventing the activity of NF-κB ameliorates dystrophic pathology in *mdx* mice, and constitutive activition of NF-κB

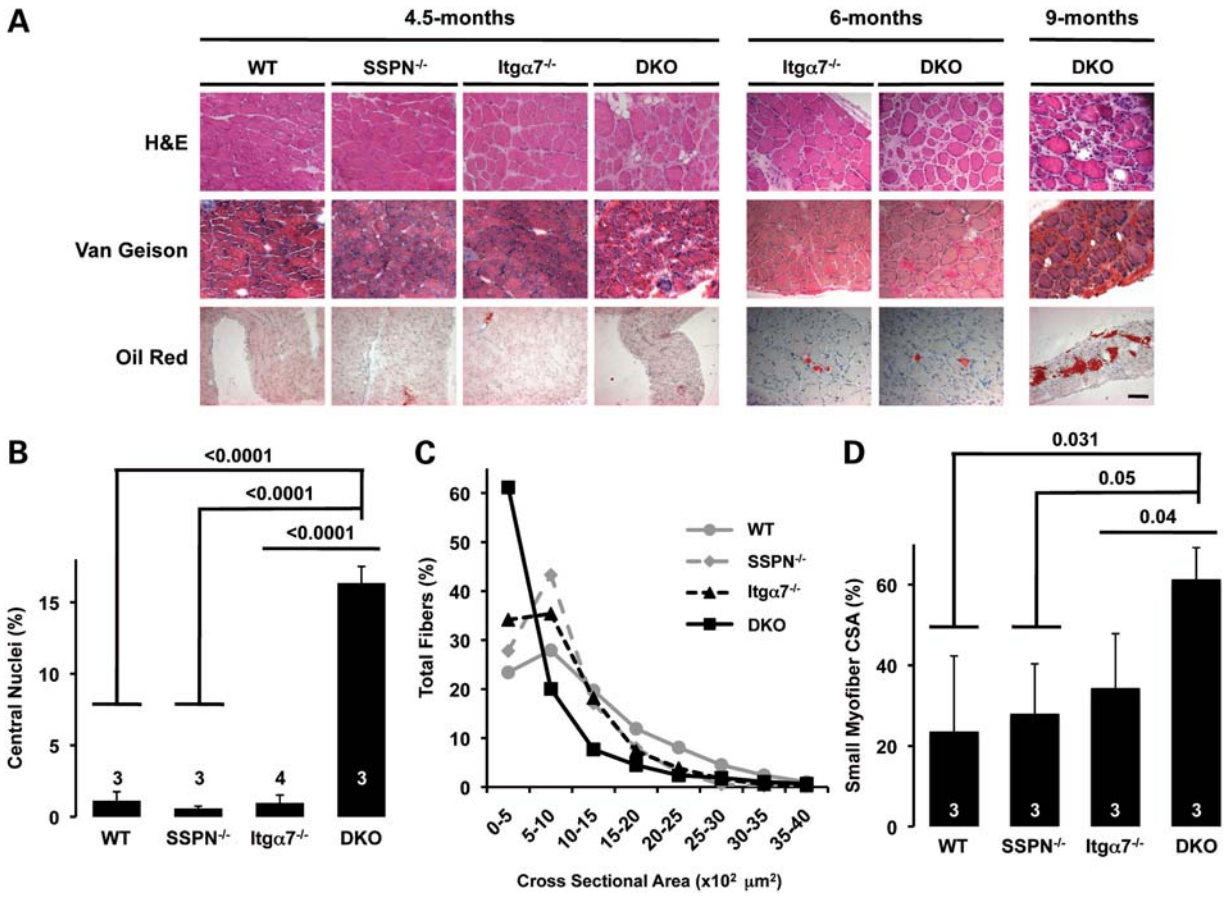

Figure 4. Increased fibrotic collagen deposition in the diaphragm of DKO mice. (**A**) Transverse cryosections of diaphragm muscle from wild-type (WT), SSPN-null (SSPN$^{-/-}$), α7 integrin-null (Itgα7$^{-/-}$) and SSPN-null:α7 integrin-null (DKO) were stained with H&E, Van Geison and Oil Red to visualize regeneration, collagen deposition and fat replacement, respectively. Age of the mice at the time of analysis is indicated. Bar, 50 μm. (**B**) Regeneration was quantified by counting central nuclei in 4.5-month-old diaphragms. Diaphragm muscles of DKO mice undergo significantly more regeneration (16-fold) compared with controls. (**C**) Myofiber CSAs of 4.5-month-old diaphragm muscles were quantified, revealing significant variation in fiber sizes in DKO muscles compared with controls. Small myofibers are prevalent in DKO ($n = 3$) diaphragm muscle compared with wild-type ($n = 3$), SSPN-null ($n = 3$) and α7 integrin-null ($n = 3$) controls. Average CSAs are plotted as an average percentage of total fibers (1400 myofibers were analyzed per diaphragm). (**D**) Graphs representing percentage of myofibers with very small CSAs (0–500 μm^2). DKO diaphragms exhibit a 2-fold increase in very small myofibers compared with all controls. Error bars represent standard deviation of the mean. Statistics were calculated using an ANOVA with a Bonferroni correction or Tukey's test. *n*- and *P*-values are indicated on the plots.

results in muscle wasting, highlighting the importance of NF-κB signaling in muscle disease (60–63). To determine whether this pathway is partly responsible for the alterations in myopathy observed in DKO muscle, we immunoblotted for the MAPK, NF-κB and MMP signaling proteins. We discovered that the additional loss of SSPN in Itgα7-deficient muscle results in greater activation of p38 MAPK, p44 MAPK and p105 NF-κB1 (Fig. 5A). Consistently, the protein levels of downstream MMP 9 were elevated (Fig. 5A). These results support a role for the MAPK–NF-κB1–MMP pathway in contributing to the exacerbated pathology observed in DKO muscle.

To determine whether the combined loss of Itgα7 and SSPN affects the localization of adhesion complexes at the sarcolemma and thus contributes to muscle pathology, indirect immunofluorescence assays were performed on transverse cryosections of quadriceps muscle from 4.5-month-old mice. Although young SSPN-deficient mice express normal levels of the DGC (32), we found a notable decrease in dystrophin, β-DG, α-SG and γ-SG and an increase in Itgα7 in aged SSPN-deficient mice (Fig. 5B). Similarly, we discovered that aged DKO muscles exhibit defects in dystrophin, DGs (α- and β-) and the SGs (α-, β- and γ-) at the sarcolemma compared with controls (Fig. 5B). Aged Itgα7-deficient mice were similar to wild-type, except that levels of α-SG were reduced at the sarcolemma (Fig. 5B). Utr was normally enriched at NMJs, although we noted a decrease in Utr in DKO muscle (Fig. 5B and C). Specificity of NMJ staining was confirmed by co-staining muscle sections with Utr antibodies and α-bungarotoxin (α-BTX) (Fig. 5C).

Enhanced Akt signaling has been shown to improve expression of the DGC, UGC and α7β1 integrin adhesion complexes, restore defective regeneration by increasing UGC expression in SSPN-deficient mice and ameliorate *mdx* pathology by improving UGC and α7β1 integrin density at the sarcolemma (51,52,64). To determine whether the combined loss of SSPN and Itgα7, in addition to suppressed Akt signaling, affected relative levels of the major adhesion complexes,

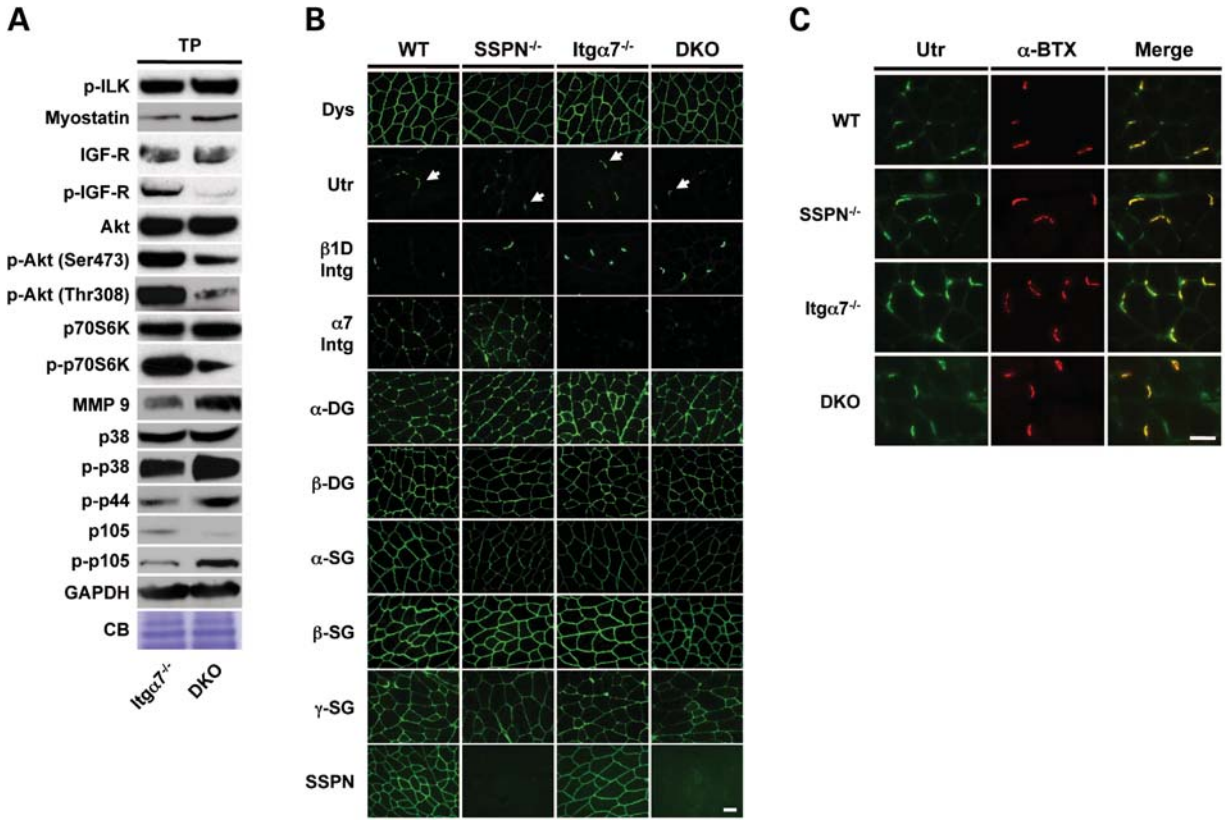

Figure 5. Loss of SSPN and α7 integrin reduces the activation of Akt and levels of the DGC and UGC. (**A**) Skeletal muscle lysates from 4.5-month-old α7 integrin-null (Itgα7$^{-/-}$) and SSPN-null:α7 integrin-null (DKO) mice were prepared in modified RIPA buffer. Equal protein samples (60 μg) were resolved by SDS–PAGE. Immunoblotting was performed with antibodies against phosphorylated ILK (p-ILK), myostatin, insulin-like growth factor receptor (IGF-R), phosphorylated IGF-R (p-IGF-R), Akt, phosphorylated Akt (p-Akt, Ser473), phosphorylated Akt (p-Akt, Thr308), p70S6K, phosphorylated p70S6K (p-p70S6K), MMP 9, p38 MAPK (p38), phosphorylated p38 MAPK (p-p38), phosphorylated p44 MAPK (p-p44), NF-κB1 p105 (p105) and phosphorylated NF-κB1 p105 (p-p105). Coomassie blue (CB) staining and GAPDH were used for loading controls. Quantification of p-Akt/Akt, p-p70S6K and p-IGF-R/IGF-R is provided in Supplementary Material, Figure S1. (**B**) Transverse cryosections of quadriceps muscle from 4.5-month-old wild-type (WT), SSPN-null (SSPN$^{-/-}$), α7 integrin-null (Itgα7$^{-/-}$) and SSPN-null:α7 integrin-null (DKO) mice were stained with antibodies against dystrophin (Dys), Utr, β1D integrin (β1D Intg), α7 integrin (α7 Intg), DGs (α- and β-DG), SGs (α-, β- and γ-SG) and SSPN. Arrows denote NMJ structures. Bar, 50 μm. (**C**) Transverse cryosections of quadriceps muscle from 4.5-month-old mice were co-stained with Utr antibody and α-BTX, which serve as a marker for NMJs. Merged images (right panels) reveal that Utr protein is localized to NMJ structures in all samples. However, NMJs in DKO muscle appear to be smaller in size with faint Utr staining. Bar, 50 μm.

protein lysates were prepared from skeletal muscle and enriched for adhesion complexes, using succinylated wheat germ agglutinin (sWGA) agarose (30). The integrity of protein interactions within macromolecular complexes was preserved using a mild digitonin buffer followed by lectin affinity chromatography, which enables a rigorous analysis of intact adhesion complexes. By immunoblotting equivalent concentrations of sWGA-enriched samples, we demonstrate that loss of SSPN decreased expression of DGC and UGC components (Fig. 6A). Furthermore, laminin binding to α-DG in SSPN-null muscle is diminished relative to wild-type as revealed by laminin overlay assays (Fig. 6A). We now provide evidence that DGC levels are reduced in aged SSPN-deficient muscle, causing reduced laminin binding. The DGC represents the major structural component of the sarcolemma and our finding that SSPN-deficiency reduces levels of dystrophin (Fig. 6A) as well as the entire DGC complex at the sarcolemma (Fig. 5B), in addition to decreasing laminin binding (Fig. 6A), is likely to have significant impact on muscle function and membrane stability.

Consistent with total skeletal protein immunoblots, β1D integrin is significantly increased in SSPN-deficient muscle compared with wild-type controls (Fig. 6A; Supplementary Material, Fig. S5C), suggesting that integrins may compensate not only for the loss of SSPN, but additionally for secondary reductions in DGC and UGC. In comparison with wild-type mice, Itgα7-deficient mice display mildly decreased levels of laminin, dystrophin, the DGs (α- and β-subunits) and laminin binding to α-DG, although Utr levels are elevated (Fig. 6A). The increase in Utr is consistent with previous reports (65).

Finally, we performed sWGA enrichments of DKO muscle to examine whether the observed reductions in laminin binding and adhesion complexes in single-null animals were further enhanced. DKO mice exhibited drastic reductions in levels of laminin and the entire DGC as well as deficits in laminin binding to α-DG (Fig. 6A). DGC/UGC proteins from sWGA enrichments are quantified in Supplementary Material, Figure S5A–I. Similar to SSPN-deficient mice, Utr levels are severely reduced in DKO mice compared with

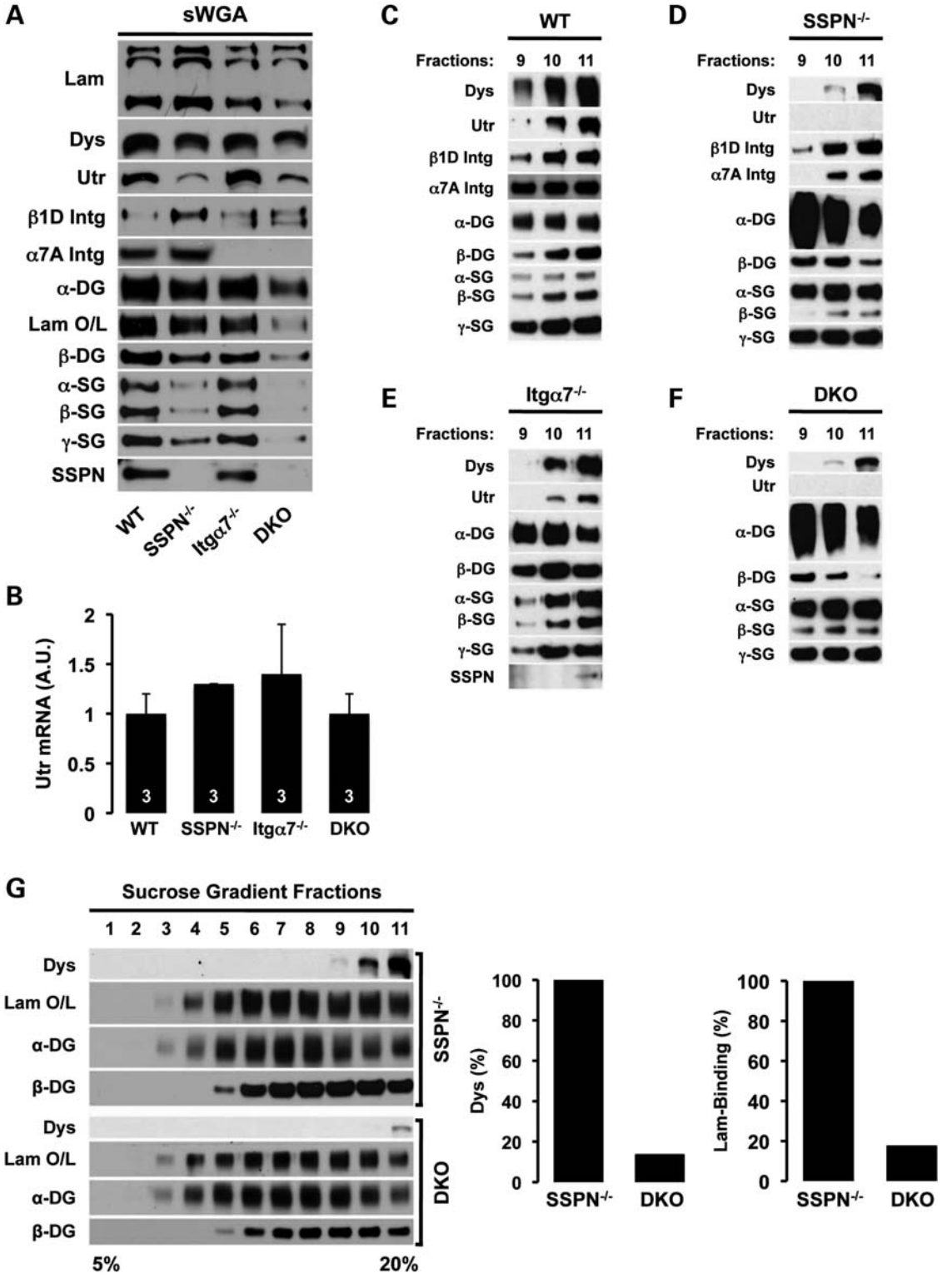

Figure 6. SSPN and integrin stabilize protein interactions within the DGC and UGC. (**A**) Skeletal muscle lysates from 4.5-month-old wild-type (WT), SSPN-null ($SSPN^{-/-}$), α7 integrin-null ($Itg\alpha7^{-/-}$) and SSPN-null:α7 integrin-null (DKO) mice were prepared in digitonin buffer and enriched by sWGA lectin chromatography. Equal protein samples (10 μg) were resolved by SDS–PAGE. Immunoblotting was performed with antibodies against laminin (Lam), dystrophin (Dys), Utr, α7 integrin (α7 Intg), β1D integrin (β1D Intg), DGs (α- and β-DG), SGs (α-, β-, γ-SG) and SSPN. Laminin protein was overlaid on α-DG and visualized by immunoblotting with antibody against laminin (Lam O/L). Quantification of lectin-purified adhesion complexes is provided in Supplementary Material, Figure S5. (**B**) Utr mRNA was measured from the quadriceps muscle of 4.5-month-old wild-type (WT), SSPN-null ($SSPN^{-/-}$), α7 integrin-null ($Itg\alpha7^{-/-}$) and SSPN-null:α7 integrin-null (DKO) mice and normalized to the GAPDH internal control. Data are presented as an average normalized to wild-type, and error bars represent standard deviation of the mean ($n = 3$ mice per genotype). Levels of Utr mRNA were not statistically altered in any genotype.

wild-type and Itgα7-null controls. Quantitative real-time PCR (qRT-PCR) analysis revealed equal quantities of Utr mRNA in all genotypes, suggesting that regulation of Utr protein occurs at the post-transcriptional level (Fig. 6B). Utr is unlikely to be a major contributor to sarcolemmal force production and stabilization since its expression is restricted to the NMJs in DKO mice (Fig. 5B and C). Therefore, exacerbated muscle pathology in DKO mice likely results from the dramatic decrease in the entire DGC and associated laminin binding capacity, in addition to reduced Akt signaling that renders the sarcolemma vulnerable to myofiber damage. Similar to SSPN-deficient mice, further reduction in the DGC, along with reduced laminin binding and loss of α7β1 integrins, is likely to have significant impact on muscle pathophysiology and strength.

The integrity of glycoprotein adhesion complexes was determined by subjecting equal concentrations of sWGA enrichments to high-speed linear sucrose centrifugation, which separates proteins by molecular mass and frictional coefficient. In wild-type muscle, all three-adhesion glycoprotein complexes migrate to fractions 9–11, which correspond to the heaviest fractions in the sucrose gradient (Fig. 6C). In agreement with previously reported data, Utr was not detectable in sucrose gradient fractions, and the DGC remains intact despite loss of SSPN (32,64). Removal of SSPN from wild-type muscle also does not alter the migration profile of α7β1 integrin (Fig. 6D). Migration of the UGC and DGC remains unchanged in comparison with wild-type profiles in Itgα7-deficient muscle (Fig. 6E). Similar to SSPN-deficient muscle, Utr was not detectable, and the DGC components remained intact in DKO fractions (Fig. 6F). To discern differences between the DKO and SSPN-deficient muscles, immunoblots of sucrose gradient fractions of SSPN-deficient and DKO mice were subjected to identical blotting conditions and exposures. Dystrophin migrates to fractions 9–11, which also contain DGs (α- and β-DG) as well as laminin-binding activity in SSPN-deficient muscle. In DKO muscle, dystrophin levels were drastically reduced and restricted to fraction 11. Additional reductions were also observed in the DGs (α- and β-DG) and laminin binding to α-DG in the dystrophin-containing fraction 11 of DKO muscle (Fig. 6G). To determine relative levels of intact DGC and laminin binding to α-DG, densitometry was performed on immunoblots shown for SSPN-deficient and DKO mice. Analysis was restricted to the dystrophin-containing fractions, and the percentage of total signal intensity of intact fractions was plotted relative to the SSPN-null controls. DKO mice exhibit an 87% reduction in dystrophin and an 83% reduction in laminin binding to α-DG compared with SSPN-deficient mice (Fig. 6G). In addition to the reductions in functional DGC, DKO mice also lack α7β1 integrin complexes, which further impacts the stability of the sarcolemma.

Loss of SSPN diminishes specific force in single-knockout and DKO mice

In order to determine whether the observed morphological and biochemical changes affected muscle function, we investigated force production in diaphragm muscle isolated from mice at 4.5 months of age. The diaphragm muscles were subjected to maximum isometric tetanus following eccentric contractions, and the average specific force and percent force drop are presented for each genotype. Diaphragms from SSPN- and Itgα7-single nulls, which possess similar reductions in laminin binding to α-DG, exhibited a 30% reduction in specific force values compared with wild-type (Fig. 7A), confirming results observed in a previous study on Itgα7-null diaphragm muscles (34). Combined loss of both SSPN and Itgα7 further reduced specific force. The effect was additive as DKO diaphragms exhibited 51% reduction in force relative to wild-type (Fig. 7A). A previous study demonstrated that SSPN-deficient extensor digitorum longus (EDL) and soleus muscles isolated from young (1 month of age) mice maintained normal force and power generation capabilities (32) and we now demonstrate that these parameters are also normal in EDL and soleus muscles from 4.5-month SSPN-nulls (Supplementary Material, Fig. S4B–E). Evaluation of muscle fragility in the diaphragm was conducted by measuring the percent drop in force between the first and fifth eccentric contraction (66). Both SSPN-deficient and DKO diaphragms exhibit increased susceptibility to eccentric contraction-induced damage as measured by the percent drop in force (Fig. 7B). Loss of Itgα7 alone did not alter the percent drop in force after eccentric contractions compared with wild-type controls, suggesting that although integrins contribute to force production, they do not contribute to membrane fragility, which is consistent with other studies (67). Our report provides evidence that aged SSPN-deficient mice exhibit impaired force production and increased susceptibility to eccentric contraction-induced injury in diaphragm muscles, demonstrating an important role for SSPN in the maintenance of muscle strength and membrane stability. Furthermore, we demonstrate that expression of both SSPN and Itgα7 is critical for normal muscle function as loss of both proteins weakens muscle, suggesting that they function in a cooperative manner.

DISCUSSION

Emerging evidence supports a model whereby SSPN interacts with each of the major adhesion complexes in skeletal muscle as a common component of laminin-binding receptors. SSPN is a core-component of the DGC and UGC (30,31). It is well established that tetraspanins interact with many transmembrane receptors, most notably the α-subunit of integrins, to regulate signaling functions. Furthermore, disruption of the

sWGA lectin enrichments from wild-type (**C**), SSPN-null (**D**), α7 integrin-null (Itgα7$^{-/-}$) (**E**) and DKO (**F**) muscle were subjected to 5–20% sucrose gradient ultracentrifugation to investigate the integrity of glycoprotein adhesion complexes. Nitrocellulose transfers were probed with the indicated antibodies. Fraction numbers from the sucrose gradients are listed above the blots. The exposures shown are not identical between different genotypes. (**G**) Sucrose gradient fractions of sWGA eluates are displayed for SSPN-null and DKO mice. All blotting and exposures were performed under identical conditions to facilitate the comparison of relative intensities for the migration profiles of dystrophin (Dys), laminin binding to α-DG (Lam O/L) and DGs (α- and β-DG). Densitometry was performed on dystrophin-containing fractions for dystrophin and laminin binding. Data are represented as total percent band intensity relative to SSPN-null band intensity. DKO mice demonstrate an 87% reduction in dystrophin protein and an 83% reduction in laminin binding to α-DG compared with SSPN-deficient controls, as shown in the plots.

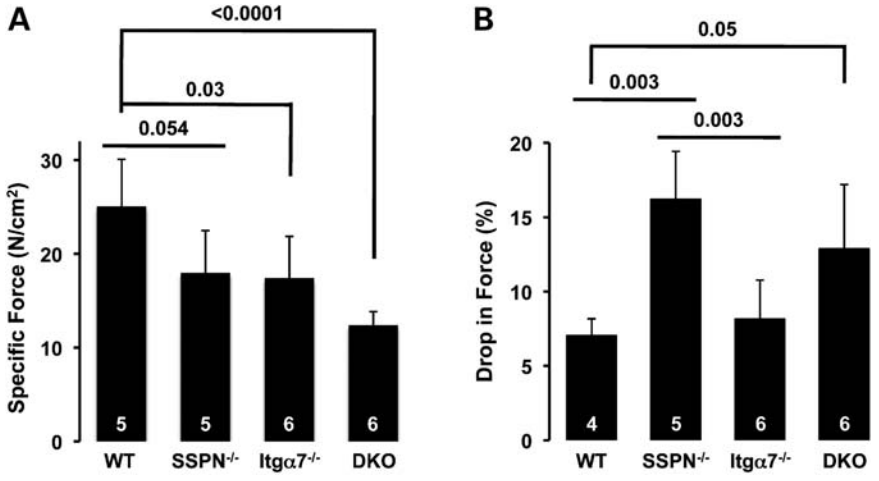

Figure 7. Specific force production is diminished in all mutant mice. (**A**) Specific force generation was measured from diaphragm muscles of 4.5-month-old wild-type (WT), SSPN-null ($SSPN^{-/-}$), α7 integrin-null ($Itg\alpha7^{-/-}$) and SSPN-null:α7 integrin-null (DKO) mice. There is a significant reduction in the generation of specific force from α7 integrin-null and DKO mice compared with wild-type controls. Data represent averages and error bars represent standard deviation of the mean. Statistics were calculated using an ANOVA with a Bonferroni correction. *n*- and *P*-values are indicated. (**B**) The percentage drop in force between the first and fifth eccentric contraction in isolated diaphragm muscles of 4.5-month-old wild-type (WT), SSPN-null ($SSPN^{-/-}$), α7 integrin-null ($Itg\alpha7^{-/-}$) and SSPN-null:α7 integrin-null (DKO) mice is plotted. The drop in force of SSPN-deficient and DKO diaphragms was significant compared with wild-type diaphragms. Data are presented as an average, and error bars represent standard deviation of the mean. Statistics were calculated using an ANOVA with a Bonferroni correction. *n*- and *P*-values are indicated on the plots.

tetraspanin–integrin association reduced the laminin-binding activity of integrins (68,69). In the current report, we investigated whether SSPN, like tetraspanins, influences the activity of α7β1 integrin, the predominantly expressed integrin in adult skeletal muscle.

We have demonstrated novel interactions between SSPN and Itgα7 that are important for maintaining expression of the DGC at the sarcolemma. Initial observations revealed that the additional loss of SSPN from Itgα7-null mice improved the embryonic lethality observed in Itgα7-null mice. We did not pursue this paradoxical discovery in the current manuscript, but it is interesting to speculate whether reduction in DKO embryonic lethality may be due to the expression of SSPN in non-muscle tissue such as the placenta or vasculature. Schematic diagrams are provided to illustrate the localization of glycoprotein adhesion complexes at the sarcolemma and their effects on laminin binding based on our analysis of lectin-enriched lysates and sucrose gradient profiles of intact complexes isolated from single- and double-null mice (Fig. 8). We show that SSPN-null mice are deficient in DGC expression and that α7β1 integrin levels are elevated to compensate for the reduction of the DGC and laminin binding. The combined removal of SSPN and Itgα7 results in undetectable levels of the UGC, similar to SSPN-deficient mice, and a reduction in the abundance of DGC complexes at the sarcolemma. The >85% reduction in the DGC results in a >80% loss of laminin-binding activity. The diminution of connections between the intracellular actin cytoskeleton and ECM renders the sarcolemma more susceptible to contraction-induced damage and results in muscle with reduced force-generating capacity, as evidenced by experiments on the diaphragm muscle. We provide evidence that SSPN interacts with α7β1 integrin at the muscle membrane, an interaction characteristic of all tetraspanins. Our data are consistent with co-immunoprecipitation experiments from cultured myotubes, suggesting that the α5β1 integrin, the embryonic form of the integrin complex, associates with the DGC (70). It is also reasonable to speculate that the pathophysiology of DKO diaphragm muscles is affected by reductions in IGF-R signaling as well as increased myostatin. Together, these molecular events contribute to decreased activation of Akt and p70S6K, resulting in reduced protein synthesis, muscle wasting and collagen accumulation giving rise to fibrosis. Similarly, the elevated levels of active MAPK and NF-κB signaling as well as MMP 9 likely contribute to the extensive necrosis and alterations in ECM deposits observed in DKO diaphragms.

The SG-SSPN subcomplex has been well described in relation to the DGC (71). Redundant functions between γ-SG and Itgα7 have been described in DKO mice displaying exacerbated myopathy, severe kyphosis and drastically shortened lifespan (72). Although the proteins levels of SSPN were not reported in γ-SG and Itgα7 DKO mice, SSPN- and Itgα7-deficient mice have reduced protein levels of the DGC, including γ-SG. γ-SG-deficient mice display muscle pathology that is more severe than SSPN-deficient mice with reduced protein levels of α- and β-SG and SSPN (73,74). Similar to SSPN-deficient mice, γ-SG-deficient mice do not exhibit deficits in the percent drop in force following eccentric contractions in the EDL muscle. It would be interesting to examine the diaphragm muscle of SG-deficient mice to determine whether reductions in force production and susceptibility to muscle damage following eccentric contractions are observed.

In addition to affecting the stability of the DGC with integrin, SSPN also determines the stability of the UGC. Over-expression of SSPN in dystrophin-deficient *mdx* mice ameliorates dystrophic pathology by stabilizing the UGC at the extra-synaptic sarcolemma (31). We have recently shown

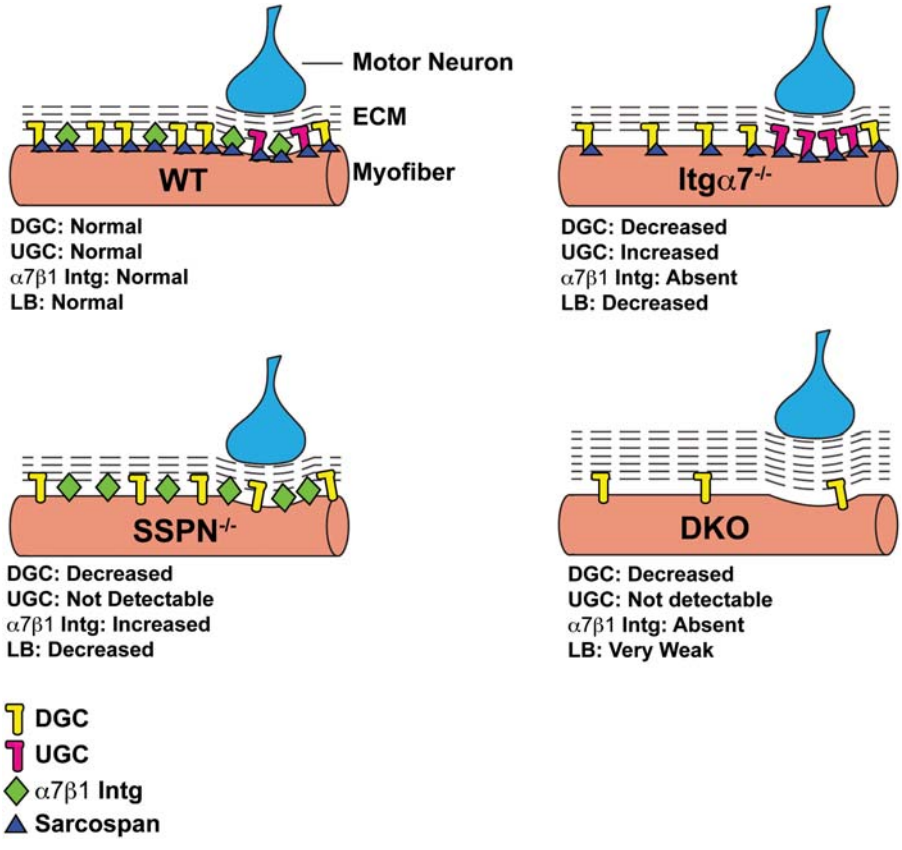

Figure 8. Effect of SSPN and α7β1 integrin on adhesion complexes in muscle. A schematic diagram is provided to illustrate the adhesion glycoprotein complexes at the sarcolemma of 4.5-month-old wild-type (WT), SSPN-null (SSPN$^{-/-}$), α7 integrin-null (Itgα7$^{-/-}$) and SSPN-null:α7 integrin-null (DKO) mice. Protein levels of the entire DGC (yellow), entire UGC (pink) and α7β1 integrin (green) complexes are described relative to wild-type muscle. The presence of SSPN is indicated with dark-blue triangles. The dashed lines represent the amount of ECM or fibrosis, and the levels of laminin binding (LB) to α-DG are described. Extra-synaptic and NMJ (where motor neuron innervates muscle) regions of the sarcolemma are depicted. The levels of the UGC and DGC are reduced in SSPN-deficient and DKO mice, and α7β1 integrin is increased in SSPN-null muscle. In DKO muscle, the increased number of dashed lines represents the increase in fibrosis observed in the diaphragm muscle. Laminin binding to α-DG is weakest in DKO muscle due to the severe reductions observed in the levels of the DGC and UGC.

that the UGC is severely reduced in SSPN-deficient mice, rendering the muscle more susceptible to cardiotoxin injury (64). Although SSPN-deficient mice were reported to display a normal muscle phenotype without force deficits (32), we recently discovered that SSPN-deficient mice exhibit reductions in the UGC and activated Akt signaling, a failure to repair efficiently after cardiotoxin injury in an Akt-dependent manner and an earlier onset of dystrophic pathology when crossed with *mdx* mice (64). These findings mimic those observed in knockouts of other tetraspanins, where the phenotype is revealed under pathological conditions such as cardiotoxin injury and dystrophin deficiency.

The reduced and restricted localization of the UGC at the NMJ in SSPN-deficient mice makes it difficult to determine whether the loss of SSPN disrupts the integrity of the UGC. To overcome this obstacle, future studies will focus on generation and analysis of SSPN-deficient *mdx* mice. Furthermore, to directly test the ability of Utr alone to alleviate symptoms of dystrophy in the *mdx* mice, we plan to generate triple-knockout mice lacking SSPN, dystrophin and Itgα7. Our studies represent the first demonstration of molecular and physiological defects resulting from the absence of SSPN and highlight the importance of interactions between SSPN and the adhesion complexes for muscle function. The use of genetic models to understand compensatory overlap between adhesion glycoprotein complexes reveals important molecular mechanisms related to the treatment of muscular dystrophy.

MATERIALS AND METHODS

Animal models

SSPN-deficient mice (32) were a generous gift from Kevin P. Campbell (University of Iowa Medical School, Iowa City, IA), and Itgα7-deficient mice (75) were transferred from UNR to UCLA. SSPN-null males were crossed to Itgα7-null homozygous females. The resulting Itgα7 heterozygous, SSPN heterozygous sibling males and females were mated to generate wild-type, SSPN-null, Itgα7-null and Itgα7-null:SSPN-null (DKO) males, which were analyzed at 18, 24 and 36 weeks of age. Genotyping protocols have been previously reported (32,75). Mice were maintained in the Life Sciences Vivarium, and all procedures were carried out in accordance with guidelines set by the Institutional

Animal Care and Use Committee at the University of California, Los Angeles.

Evans blue dye assay

Sarcolemma membrane damage was assessed using an EBD tracer analysis that was performed by an intraperitoneal injection of mice with 50 μl of EBD (10 mg/ml in 10 mM of sterile phosphate buffer and 150 mM NaCl, pH 7.4) per 10 g of body weight at least 8 h prior to dissection as described previously (45). Quadriceps muscles were processed as described below.

Immunofluorescence assays

Muscles were mounted in 10.2% polyvinyl alcohol/4.3% polyethylene glycol and flash-frozen in liquid nitrogen-cooled isopentane. Muscles were stored at −80°C until further processing. Transverse sections (8 μm) were placed onto positively charged glass slides (Thermo Fisher Scientific) and stored at −80°C. Sections were acclimated to room temperature for 15 min and blocked with 3% BSA diluted in PBS for 30 min at room temperature. The avidin/biotin blocking kit (Vector Labs) was used according to manufacturer's instructions. Mouse primary antibodies were prepared with the M.O.M. blocking reagent (Vector Labs) as described by the manufacturer's protocol. Sections were incubated in primary antibody in PBS at 4°C overnight with the following antibodies: dystrophin (MANDYS1, 1:5; Development Studies Hybridoma Bank), Utr (MANCHO3, 1:5; Development Studies Hybridoma Bank), α-DG IIH6 (sc-53987, 1:500; Santa Cruz Biotechnology, Inc.), β-DG (MANDAG2, 1:50; Development Studies Hybridoma Bank), α-SG (VP-A105, 1:30; Vector Labs), β-SG (VP-B206, 1:30; Vector Labs), γ-SG (VP-G803, 1:30; Vector Labs), laminin (L9393, 1:25; Sigma), β1D integrin (MAB1900, 1:20; Chemicon), α7A integrin (affinity purified, rabbit A2 345, 1:500) (23), eMHC (F1.652, 1:25; Developmental Studies Hybridoma Bank), α-BTX conjugated to AlexaFluor® 555 (B35451, 1:200; Molecular Probes™) and SSPN (affinity purified rabbit 18, 1:200). Polyclonal antibodies to endogenous mouse SSPN have been described previously (76). Primary antibodies were detected by biotinylated anti-rabbit (BA-1000, 1:500; Vector Labs), fluorescein anti-IGM (AP128F, 1:500, Chemicon) and biotinylated anti-mouse (BA-9200, 1:500; Vector Labs). Fluorescein (A-2001, 1:500; Vector Labs)-conjugated avidin D was used to detect biotinylated secondary antibodies. Both secondary and tertiary probes were diluted in PBS and incubated with sections for 1 h at room temperature. Sections were mounted in VECTASHIELD (Vector Labs) to prevent photobleaching. Sections were incubated with secondary and tertiary antibodies alone as a control for specificity. Antibody-stained sections were visualized using a fluorescent microscope (Axioplan 2; Carl Zeiss, Inc.) equipped with a Plan Neofluar 40× NA 1.3 oil differential interference contrast objective, and images were captured under identical conditions using the Axiovision Rel 4.5 software (Carl Zeiss, Inc.).

Histology

H&E staining was used for the visualization of centrally placed nuclei as described previously (77). Transverse quadriceps and diaphragm sections (8 μm) were acclimated to room temperature for 15 min before beginning the staining procedure. Slides were incubated in hematoxylin for 5 min, washed in water for 2 min, incubated in eosin for 5 min and dehydrated in 70, 80, 90 and 100% ethanol. Sections were then incubated in xylene for 10 min and mounted in Permount. All supplies for this procedure were purchased from Thermo Fisher Scientific. Van Geison staining (adapted from 78) was used to compare collagen infiltration around transverse muscle fibers. Slides were incubated for 5 min in Celestin Blue (206342, Sigma-Aldrich) diluted in 5% ammonium ferric sulfate (221260, Sigma-Aldrich), rinsed with distilled water, incubated for 5 min in hematoxylin, rinsed in distilled water, incubated for 5 min in Curtis stain and dehydrated in 70, 80, 90 and 100% ethanol. Sections were then incubated in xylene for 10 min and mounted in Permount. Oil Red staining was performed according to instructions in the NovaUltra Oil Red O Stain Kit (IW-3008, IHCWORLD). Images of quadriceps/diaphragms were captured under identical conditions using an Axioplan 2 fluorescent microscope equipped with a Plan Neofluar 40× NI 1.3 oil differential interference contrast objective and the Axiovision Rel 4.5 software (Carl Zeiss, Inc.). The percentage of centrally nucleated fibers was assessed from three to four quadriceps/diaphragms of each genotype. The data are represented as an average percentage of the total number of fibers in each whole-muscle section.

Protein preparation from skeletal muscle

Total skeletal muscle was snap-frozen in liquid nitrogen and stored at −80°C. Tissues were ground to a fine powder using a mortar and pestle and then added to ice-cold radioimmunoprecipitation assay buffer (RIPA) (89901; Thermo Scientific) with phosphatase inhibitors (78420; Thermo Scientific) or DGC buffer (50 mM Tris–HCl, pH 7.8, 500 mM NaCl and 0.1% digitonin) containing fresh protease inhibitors (0.6 μg/ml pepstatin A, 0.5 μg/ml aprotinin, 0.5 μg/ml leupeptin, 0.75 mM benzamidine, 0.2 mM PMSF, 5 μM calpain I and 5 μM calpeptin). Homogenates were rotated at 4°C for 1 h. Lysates were clarified by centrifugation at 15 000*g* for 20 min at 4°C, protein concentration was determined using the DC Protein Assay (Bio-Rad) and lysates were stored at −80°C.

Immunoblot analysis

Equal quantities (10 μg for sWGA and 60 μg for total protein) of protein samples were resolved on 4–20% Pierce precise protein gels (Thermo Scientific) by SDS–PAGE and transferred to nitrocellulose membranes (Millipore). An identical protein gel was stained with Coomassie blue stain to visualize levels of total protein. 5% BLOTTO (non-fat dry milk in TBS with 0.2% Tween-20) was used to block membranes for 30 min at room temperature and incubate in primary antibodies overnight at 4°C. Incubations were performed with the following primary antibodies: dystrophin (MANDYS1,

1:200; Development Studies Hybridoma Bank), Utr (MANCHO3, 1:50; Development Studies Hybridoma Bank), α-DG IIH6 (sc-53987, 1:500; Santa Cruz Biotechnology, Inc.), β-DG (MANDAG2, 1:250; Development Studies Hybridoma Bank), α-SG (VP-A105, 1:100; Vector Labs), β-SG (VP-B206, 1:100; Vector Labs), γ-SG (VP-G803, 1:100; Vector Labs), laminin (L9393, 1:5000; Sigma), β1D integrin (MAB1900, 1:200; Chemicon), α7A integrin (affinity purified, rabbit A2 345, 1:500) (23), Akt (9272, 1:750; Cell Signaling Technology), phospho-Akt (Ser473) (9271, 1:750; Cell Signaling Technology), phospho-Akt (Thr308) (2965, 1:1000; Cell Signaling Technology), p70S6K (9202, 1:250; Cell Signaling Technology), phospho-p70S6K (Thr389) (9336, 1:500; Cell Signaling Technology), IGF-R (3027, 1:750; Cell Signaling Technology), phospho-IGF-R (Tyr1135/1136, 3024, 1:1000; Cell Signaling Technology), phospho-ILK (Ser246, AB1076, 1:1000; Millipore), myostatin (ab996, 1:500; Abcam), MMP 9 (AF909, 1:1000; R&D Systems), p38 MAPK (9212, 1:1000; Cell Signaling Technology), phospho-p38 MAPK (Thr180/Tyr182, 9216, 1:2000; Cell Signaling Technology), phospho-p44/42 MAPK (Thr202/Tyr204, 8544, 1:1000; Cell Signaling Technology), NF-κB1 p105 (4717, 1:1000; Cell Signaling Technology), phospho-NF-κB1 p105 (Ser933, 4806, 1:1000; Cell Signaling Technology), SSPN (affinity purified, rabbit 3, 1:5) and GAPDH (MAB374, 1:50 000; Chemicon). Coomassie blue staining was used as an additional loading control. Horseradish peroxidase-conjugated anti-rabbit IgG (GE Healthcare), anti-mouse IgG (GE Healthcare) and anti-mouse IgM (Roche) secondary antibodies were used at 1:2000 dilutions in 5% BLOTTO and incubated at room temperature for 3 h. Immunoblots were developed using enhanced chemiluminescence (SuperSignal West Pico Chemiluminescent Substrate; Thermo Scientific). Densitometry was quantified using an Alphaimager 2200 (Alpha Innotech). Autorads were exposed to white light and the protein of interest was boxed. The same area was used for all blots from the same experiment for consistency. The average integrated density value was recorded and normalized to controls.

sWGA enrichment and sucrose gradient ultracentrifugation

Protein samples (7 mg) were incubated with 1.2 ml of succinylated WGA-conjugated agarose slurry (AL-1023S, Vector labs) and gently rotated overnight at 4°C. sWGA agarose was washed four times in 10 ml of cold DGC solubilization buffer (50 mM Tris–HCl, pH 7.8, 500 mM NaCl and 0.1% digitonin) containing fresh protease inhibitors (0.6 μg/ml pepstatin A, 0.5 μg/ml aprotinin, 0.5 μg/ml leupeptin, 0.75 mM benzamidine, 0.2 mM PMSF, 5 μM calpain I and 5 μM calpeptin) to remove unbound proteins. Bound proteins were eluted with 0.3 M *N*-acetylglucosamine (sWGA) (Sigma-Aldrich) and concentrated using Centricon Ultracel filtration columns (Millipore) by centrifugation at 4000*g* for 75 min. Protein concentration was determined with the DC Protein Assay (Bio-Rad). Equal concentrations of eluates (10 μg) were resolved by SDS–PAGE, transferred to nitrocellulose membranes and immunoblotted as described earlier. Samples of sWGA enrichments (200 μg) were loaded on a 5–20% sucrose gradient column. The column was prepared by adding 6 ml of 5% sucrose solution into an open-top polyclear centrifuge tube (7030, Seton), using a 14-guage Hamilton syringe and underlaying with an equal volume of 20% sucrose solution. Gradients were mixed using the Gradient IP station (Biocomp). Sucrose gradients were centrifuged overnight at 4°C at 35 000*g* in an ultra-centrifuge (Optima L-90K; Beckman Coulter), using an SW41 rotor (Beckman Coulter). Twelve 1 ml fractions were collected and concentrated at 14 000*g* at 4°C for 2.5 h, using Amicon Ultra-0.5 filters (UFC500324, Millipore). Each fraction (18 μl) was resolved by SDS–PAGE, transferred to nitrocellulose membranes and immunoblotted as described in the previous section.

Laminin overlay assay

Membranes were prepared as described in sWGA enrichment of protein lysates and blocked with 5% BSA in laminin-binding buffer (LBB; 10 mM triethanolamine, 140 mM NaCl, 1 mM $MgCl_2$, 1 mM $CaCl_2$, pH 7.6) followed by incubation of mouse ultrapure Engelbreth–Holm–Swarm laminin (354239, BD Biosciences) in LBB for 6 h at 4°C. Membranes were washed and incubated with rabbit anti-laminin (L9393, 1:5000; Sigma) overnight at 4°C followed by horseradish peroxidase-conjugated anti-rabbit IgG or anti-mouse IgG (GE Healthcare) at room temperature for 3 h. Blots were developed by enhanced chemiluminescence (SuperSignal West Pico Chemiluminescent Substrate; Thermo Scientific).

Quantitative RT-PCR

The RNeasy Fibrous Tissue Kit (Qiagen, Valencia, CA, USA) was used according to the manufacturer's instructions to isolate total RNA from quadriceps of 3–6-week-old mice. Dissected muscles were stored in RNA*later* (Ambion, Austin, TX, USA). RNA integrity was verified by visualization of RNA after electrophoresis through agarose. RNA concentrations were determined using a NanoDrop 1000 instrument (Thermo Scientific, Wilmington, DE, USA). Reverse transcription was performed using the Maxima^{TM} First Strand cDNA Synthesis Kit (Fermentas, Inc.) with 3 μg of total RNA following the recommendations of the manufacturer. qRT-PCR was performed in triplicates on a TaqMan ABI PRISM 7900 (Applied Biosystems) according to the instructions in the Maxima^{TM} SYBR Green Kit (Fermentas, Inc.). GAPDH mRNA was used as an internal control. PCR conditions and primers for Utr have been described previously (31,79). Relative gene expression was quantified by the $2^{-\Delta\Delta CT}$ method.

Specific force measurements

The contractile properties of the diaphragm, EDL and soleus muscles were measured as described previously (66). After mice were anesthetized with ketamine/xylazine (80 and 10 mg/kg body weight, respectively), muscles were dissected, removed and placed in a bath of Ringer's solution gas-equilibrated with 95% O_2/5% CO_2. Sutures were attached to the central tendon and the rib in the diaphragm preparations.

Muscles were subjected to isolated mechanical measurements, using a previously described apparatus (Aurora Scientific, Ontario, Canada) (80). After determining optimum length (Lo) by supramaximal twitch stimulation, maximum isometric tetanus was measured. Upon completion of these measurements, muscles were then subjected to a series of five eccentric contractions with a 5 min rest between contractions. Average specific force of maximal isometric tetanus was displayed per genotype. Susceptibility to eccentric contraction-induced injury was measured by calculating the percent drop in force between the first and the last contraction. Other EDL muscles were stimulated once per second for 10 min (200 μs pulse, 100 Hz, 330 ms duration) in order to determine resistance to fatigue. Plots contain standard deviation, *n*-values and *P*-values calculated by performing an analysis of variance (ANOVA) with Bonferroni's correction or Tukey's multiple comparison tests to determine significance. Upon completion of analysis, muscles were rapidly frozen in OCT Quadriceps, EDL, soleus and tibialis anterior, and gastrocnemius muscles were dissected from the same mice and muscle weights were recorded. Additionally, body weight of each mouse was recorded prior to beginning the dissections. Data were analyzed by determining average muscle weight per genotype, calculating standard deviation and performing an ANOVA with Bonferroni's correction or Tukey's multiple comparison tests to determine significance.

Statistics

All statistics were analyzed using the one-way ANOVA with a Bonferroni correction or Tukey's multiple comparison tests to determine differences between groups. *n*- and *P*-values are indicated on the plots. Statistical significance was accepted for $P < 0.05$.

SUPPLEMENTARY MATERIAL

Supplementary Material is available at *HMG* online.

ACKNOWLEDGEMENTS

The authors thank B. Burton, E. Canales, S. Clark, A. Grossi, M.P. Huang and A. Ocampo for technical expertise; Dr E.R. Barton, Z. Tian and the Paul Wellstone Muscular Dystrophy Cooperative Research Center of the National Institutes of Health (U54 AR052646 to H.L.S. and E.R.B.) at the University of Pennsylvania for specific force measurements; Dr D.J. Hoelzle for assistance with statistical analysis; and Dr T. Kitada for critically reading the manuscript.

Conflict of Interest statement. None declared.

FUNDING

This work was supported by grants from the Genetic Mechanisms Pre-doctoral Training Fellowship USPHS National Research Service Award (GM07104), the Edith Hyde Fellowship, and the Eureka Pre-doctoral Training Fellowship to J.L.M.; Undergraduate Research Fellows Program to E.C.; Undergraduate Research Fellows Program to J.O.; National Institutes of Health/National Institute of Arthritis and Musculoskeletal and Skin (R01 AR053697 to D.J.B.); and National Institutes of Health/National Institute of Arthritis and Musculoskeletal and Skin (R01 AR048179 to R.H.C.-W.).

REFERENCES

1. Bonnemann, C.G. and Finkel, R.S. (2002) Sarcolemmal proteins and the spectrum of limb-girdle muscular dystrophies. *Semin. Pediatr. Neurol.*, **9**, 81–99.
2. Carmignac, V. and Durbeej, M. (2012) Cell-matrix interactions in muscle disease. *J. Pathol.*, **226**, 200–218.
3. Ervasti, J.M. (2007) Dystrophin, its interactions with other proteins, and implications for muscular dystrophy. *Biochem. Biophys. Acta*, **1772**, 108–117.
4. Ibraghimov-Beskrovnaya, O., Ervasti, J.M., Leveille, C.J., Slaughter, C.A., Sernett, S.W. and Campbell, K.P. (1992) Primary structure of dystrophin-associated glycoproteins linking dystrophin to the extracellular matrix. *Nature*, **355**, 696–702.
5. Ibraghimov-Beskrovnaya, O., Milatovich, A., Ozcelik, T., Yang, B., Koepnick, K., Francke, U. and Campbell, K.P. (1993) Human dystroglycan: skeletal muscle cDNA, genomic structure, origin of tissue specific isoforms and chromosomal localization. *Hum. Mol. Genet.*, **2**, 1651–1657.
6. Khurana, T.S., Watkins, S.C., Chafey, P., Chelly, J., Tome, F.M., Fardeau, M., Kaplan, J.C. and Kunkel, L.M. (1991) Immunolocalization and developmental expression of dystrophin related protein in skeletal muscle. *Neuromuscul. Disord.*, **1**, 185–194.
7. Love, D.R., Hill, D.F., Dickson, G., Spurr, N.K., Byth, B.C., Marsden, R.F., Walsh, F.S., Edwards, Y.H. and Davies, K.E. (1989) An autosomal transcript in skeletal muscle with homology to dystrophin. *Nature*, **339**, 55–58.
8. Matsumura, K., Ervasti, J.M., Ohlendieck, K., Kahl, S.D. and Campbell, K.P. (1992) Association of dystrophin-related protein with dystrophin-associated proteins in mdx mouse muscle. *Nature*, **360**, 588–591.
9. Bao, Z.Z., Lakonishok, M., Kaufman, S. and Horwitz, A.F. (1993) Alpha 7 beta 1 integrin is a component of the myotendinous junction on skeletal muscle. *J. Cell Sci.*, **106**, 579–589.
10. Yao, C.C., Ziolber, B.L., Squillace, R.M. and Kramer, R.H. (1996) Alpha7 integrin mediates cell adhesion and migration on specific laminin isoforms. *J. Biol. Chem.*, **271**, 25598–25603.
11. Collo, G., Starr, L. and Quaranta, V. (1993) A new isoform of the laminin receptor integrin alpha 7 beta 1 is developmentally regulated in skeletal muscle. *J. Biol. Chem.*, **268**, 19019–19024.
12. Martin, P.T., Kaufman, S.J., Kramer, R.H. and Sanes, J.R. (1996) Synaptic integrins in developing, adult, and mutant muscle: selective association of alpha1, alpha7A, and alpha7B integrins with the neuromuscular junction. *Dev. Biol.*, **174**, 125–139.
13. Song, W.K., Wang, W., Foster, R.F., Bielser, D.A. and Kaufman, S.J. (1992) H36-alpha 7 is a novel integrin alpha chain that is developmentally regulated during skeletal myogenesis. *J. Cell Biol.*, **117**, 643–657.
14. Bulfield, G., Siller, W.G., Wright, P.A. and Moore, K.J. (1984) X choromosome-linked muscular dystrophy (*mdx*) in the mouse. *Proc. Natl Acad. Sci. USA*, **81**, 1189–1192.
15. Carnwath, J.W. and Shotton, D.M. (1987) Muscular dystrophy in the *mdx* mouse: histopathology of the soleus and extensor digitorum longus muscles. *J. Neurol. Sci.*, **80**, 39–54.
16. Hodges, B.L., Hayashi, Y.K., Nonaka, I., Wang, W., Arahata, K. and Kaufman, S.J. (1997) Altered expression of the alpha7beta1 integrin in human and murine muscular dystrophies. *J. Cell Sci.*, **110**, 2873–2881.
17. Pons, F., Robert, A., Fabbrizio, E., Hugon, G., Califano, J.C., Fehrentz, J.A., Martinez, J. and Mornet, D. (1994) Utrophin localization in normal and dystrophin-deficient heart. *Circulation*, **90**, 369–374.
18. Tanabe, Y., Esaki, K. and Nomura, T. (1986) Skeletal muscle pathology in X chromosome-linked muscular dystrophy (mdx) mouse. *Acta Neuropathol.*, **69**, 91–95.
19. Tanaka, H., Ishiguro, T., Eguchi, C., Saito, K. and Ozawa, E. (1991) Expression of a dystrophin-related protein associated with the skeletal muscle cell membrane. *Histochemistry*, **96**, 1–5.

20. Deconinck, A.E., Rafael, J.A., Skinner, J.A., Brown, S.C., Potter, A.C., Metzinger, L., Watt, D.J., Dickson, J.G., Tinsley, J.M. and Davies, K.E. (1997) Utrophin-dystrophin deficient mice as a model for Duchenne muscular dystrophy. *Cell*, **90**, 717–727.
21. Grady, R.M., Teng, H., Nichol, M.C., Cuttingham, J.C., Wilkinson, R.S. and Sanes, J.R. (1997) Skeletal and cardiac myopathies in mice lacking utrophin and dystrophin: a model for Duchenne muscular dystrophy. *Cell*, **90**, 729–738.
22. Guo, C., Willem, M., Werner, A., Raivich, G., Emerson, M., Neyses, L. and Mayer, U. (2006) Absence of alpha 7 integrin in dystrophin-deficient mice causes a myopathy similar to Duchenne muscular dystrophy. *Hum. Mol. Genet.*, **15**, 989–998.
23. Rooney, J.E., Welser, J.V., Dechert, M.A., Flintoff-Dye, N.L., Kaufman, S.J. and Burkin, D.J. (2006) Severe muscular dystrophy in mice that lack dystrophin and alpha7 integrin. *J. Cell Sci.*, **119**, 2185–2195.
24. Burkin, D.J., Wallace, G.Q., Milner, D.J., Chaney, E.J., Mulligan, J.A. and Kaufman, S.J. (2005) Transgenic expression of alpha7beta1 integrin maintains muscle integrity, increases regenerative capacity, promotes hypertrophy, and reduces cardiomyopathy in dystrophic mice. *Am. J. Pathol.*, **166**, 253–263.
25. Burkin, D.J., Wallace, G.Q., Nicol, K.J., Kaufman, D.J. and Kaufman, S.J. (2001) Enhanced expression of the alpha 7 beta 1 integrin reduces muscular dystrophy and restores viability in dystrophic mice. *J. Cell Biol.*, **152**, 1207–1218.
26. Gilbert, R., Nalbanoglu, J., Tinsley, J.M., Massie, B., Davies, K.E. and Karpati, G. (1998) Efficient utrophin expression following adenovirus gene transfer in dystrophic muscle. *Biochem. Biophys. Res. Commun.*, **242**, 244–247.
27. Liu, J., Milner, D.J., Boppart, M.D., Ross, R.S. and Kaufman, S.J. (2012) beta1D chain increases alpha7beta1 integrin and laminin and protects against sarcolemmal damage in *mdx* mice. *Hum. Mol. Genet.*, **21**, 1592–1603.
28. Tinsley, J., Deconinck, N., Risher, R., Kahn, D., Phelps, S., Gillis, J.M. and Davies, K. (1998) Expression of full-length utrophin prevents muscular dystrophy in *mdx* mice. *Nat. Med.*, **4**, 1441–1444.
29. Tinsley, J.M., Potter, A.C., Phelps, S.R., Fisher, R., Trickett, J.I. and Davies, K.E. (1996) Amelioration of the dystrophic phenotype of *mdx* mice using a truncated utrophin transgene. *Nature*, **384**, 349–353.
30. Crosbie, R.H., Heighway, J., Venzke, D.P., Lee, J.C. and Campbell, K.P. (1997) Sarcospan, the 25-kDa transmembrane component of the dystrophin-glycoprotein complex. *J. Biol. Chem.*, **272**, 31221–31224.
31. Peter, A.K., Marshall, J.L. and Crosbie, R.H. (2008) Sarcospan reduces dystrophic pathology: stabilization of the utrophin-glycoprotein complex. *J. Cell Biol.*, **183**, 419–427.
32. Lebakken, C.S., Venzke, D.P., Hrstka, R.F., Consolino, C.M., Faulkner, J.A., Williamson, R.A. and Campbell, K.P. (2000) Sarcospan-deficient mice maintain normal muscle function. *Mol. Cell Biol.*, **20**, 1669–1677.
33. Mayer, U., Saher, G., Fassler, R., Bornemann, A., Echtermeyer, F., von der Mark, H., Miosge, N., Poschl, E. and von der Mark, K. (1997) Absence of integrin alpha 7 causes a novel form of muscular dystrophy. *Nat. Genet.*, **17**, 318–323.
34. Lopez, M.A., Mayer, U., Hwang, W., Taylor, T., Hashmi, M.A., Jannapureddy, S.R. and Boriek, A.M. (2005) Force transmission, compliance, and viscoelasticity are altered in the alpha7-integrin-null mouse diaphragm. *Am. J. Physiol. Cell Physiol.*, **288**, C282–C289.
35. Burkin, D.J., Gu, M., Hodges, B.L., Campanelli, J.T. and Kaufman, S.J. (1998) A functional role for specific spliced variants of the alpha7beta1 integrin in acetylcholine receptor clustering. *J. Cell Biol.*, **143**, 1067–1075.
36. Burkin, D.J., Kim, J.E., Gu, M. and Kaufman, S.J. (2000) Laminin and alpha7beta1 integrin regulate agrin-induced clustering of acetylcholine receptors. *J. Cell Sci.*, **113**, 2877–2886.
37. Nawrotzki, R., Willem, M., Miosge, N., Brinkmeier, H. and Mayer, U. (2003) Defective integrin switch and matrix composition at alpha 7-deficient myotendinous junctions precede the onset of muscular dystrophy in mice. *Hum. Mol. Genet.*, **12**, 483–495.
38. Takemitsu, M., Ishiura, S., Koga, R., Kamakura, K., Arahata, K., Nonaka, I. and Sugita, H. (1991) Dystrophin-related protein in the fetal and denervated skeletal muscles of normal and *mdx* mice. *Biochem. Biophys. Res. Commun.*, **180**, 1179–1186.
39. Pons, F., Augier, N., Léger, J.O., Robert, A., Tomé, F.M., Fardeau, M., Voit, T., Nicholson, L.V., Mornet, D. and Léger, J.J. (1991) A homologue of dystrophin is expressed at the neuromuscular junctions of normal individuals and DMD patients, and of normal and *mdx* mice. Immunological evidence. *FEBS Lett.*, **282**, 161–165.
40. Voit, T., Haas, K., Léger, J.O., Pons, F. and Léger, J.J. (1991) Xp21 dystrophin and 6q dystrophin-related protein. Comparative immunolocalization using multiple antibodies. *Am. J. Pathol.*, **139**, 969–976.
41. Nguyen, T.M., Ellis, J.M., Love, D.R., Davies, K.E., Gatter, K.C., Dickson, G. and Morris, G.E. (1991) Localization of the DMDL gene-encoded dystrophin-related protein using a panel of nineteen monoclonal antibodies: presence at neuromuscular junctions, in the sarcolemma of dystrophic skeletal muscle, in vascular and other smooth muscles, and in proliferating brain cell lines. *J. Cell Biol.*, **115**, 1695–1700.
42. Welser, J.V., Lange, N., Singer, C.A., Elorza, M., Scowen, P., Keef, K.D., Gerthoffer, W.T. and Burkin, D.J. (2007) Loss of the alpha7 integrin promotes extracellular signal-regulated kinase activation and altered vascular remodeling. *Circ. Res.*, **101**, 672–681.
43. Laws, N. and Hoey, A. (2004) Progression of kyphosis in mdx mice. *J. Appl. Physiol.*, **97**, 1970–1977.
44. Manzur, A.Y. and Muntoni, F. (2009) Diagnosis and new treatments in muscular dystrophies. *Postgrad. Med. J.*, **85**, 622–630.
45. Straub, V., Rafael, J.A., Chamberlain, J.S. and Campbell, K.P. (1997) Animal models for muscular dystrophy show different patterns of sarcolemmal disruption. *J. Cell Biol.*, **139**, 375–385.
46. Stedman, H.H., Sweeney, H.L., Shrager, J.B., Maguire, H.C., Panettieri, R.A., Petrof, B., Narusawa, M., Leferovich, J.M., Sladky, J.T. and Kelly, A.M. (1991) The mdx mouse diaphragm reproduces the degenerative changes of Duchenne muscular dystrophy. *Nature*, **352**, 536–539.
47. Glass, D. and Roubenoff, R. (2011) Recent advances in the biology and therapy of muscle wasting. *Ann. NY Acad. Sci.*, **1211**, 25–36.
48. Otto, A. and Patel, K. (2010) Signalling and the control of skeletal muscle size. *Exp. Cell Res.*, **316**, 3059–3066.
49. Wang, H.V., Chang, L.W., Brixius, K., Wickstrom, S.A., Montanez, E., Thievessen, I., Schwander, M., Muller, U., Bloch, W., Mayer, U. and Fassler, R. (2008) Integrin-linked kinase stabilizes myotendinous junctions and protects muscle from stress-induced damage. *J. Cell Biol.*, **180**, 1037–1049.
50. Peng, X.D., Xu, P.Z., Chen, M.L., Hahn-Windgassen, A., Skeen, J., Jacobs, J., Sundararajan, D., Chen, W.S., Crawford, S.E., Coleman, K.G. and Hay, N. (2003) Dwarfism, impaired skin development, skeletal muscle atrophy, delayed bone development, and impeded adipogenesis in mice lacking Akt1 and Akt2. *Genes Dev.*, **17**, 1352–1365.
51. Peter, A.K., Ko, C.Y., Kim, M.H., Hsu, N., Ouchi, N., Rhie, S., Izumiya, Y., Zeng, L., Walsh, K. and Crosbie, R.H. (2009) Myogenic Akt signaling upregulates the utrophin-glycoprotein complex and promotes sarcolemma stability in muscular dystrophy. *Hum. Mol. Genet.*, **18**, 318–327.
52. Kim, M.H., Kay, D.I., Rudra, R.T., Chen, B.M., Hsu, N., Izumiya, Y., Martinez, L., Spencer, M.J., Walsh, K., Grinnell, A.D. and Crosbie, R.H. (2011) Myogenic Akt signaling attenuates muscular degeneration, promotes myofiber regeneration and improves muscle function in dystrophin-deficient mdx mice. *Hum. Mol. Genet.*, **20**, 1324–1338.
53. Trendelenburg, A.U., Meyer, A., Rohner, D., Boyle, J., Hatakeyama, S. and Glass, D.J. (2009) Myostatin reduces Akt/TORC1/p70S6K signaling, inhibiting myoblast differentiation and myotube size. *Am. J. Physiol. Cell Physiol.*, **296**, C1258–C1270.
54. Barton, E.R., Morris, L., Musaro, A., Rosenthal, N. and Sweeney, H.L. (2002) Muscle-specific expression of insulin-like growth factor I counters muscle decline in *mdx* mice. *J. Cell Biol.*, **157**, 137–148.
55. Musaro, A., McCullagh, K., Paul, A., Houghton, L., Dobrowolny, G., Molinaro, M., Barton, E.R., Sweeney, H.L. and Rosenthal, N. (2001) Localized Igf-1 transgene expression sustains hypertrophy and regeneration in senescent skeletal muscle. *Nat. Genet.*, **27**, 195–200.
56. Scicchitano, B.M., Rizzuto, E. and Musaro, A. (2009) Counteracting muscle wasting in aging and neuromuscular diseases: the critical role of IGF-1. *Aging (Albany NY)*, **1**, 451–457.
57. Dahiya, S., Bhatnagar, S., Hindi, S.M., Jiang, C., Paul, P.K., Kuang, S. and Kumar, A. (2011) Elevated levels of active matrix metalloproteinase-9 cause hypertrophy in skeletal muscle of normal and dystrophin-deficient mdx mice. *Hum. Mol. Genet.*, **20**, 4345–4359.
58. Kherif, S., Lafuma, C., Dehaupas, M., Lachkar, S., Fournier, J.G., Verdiere-Sahuque, M., Fardeau, M. and Alameddine, H.S. (1999) Expression of matrix metalloproteinases 2 and 9 in regenerating skeletal

muscle: a study in experimentally injured and mdx muscles. *Dev. Biol.*, **205**, 158–170.
59. Li, H., Mittal, A., Makonchuk, D.Y., Bhatnagar, S. and Kumar, A. (2009) Matrix metalloproteinase-9 inhibition ameliorates pathogenesis and improves skeletal muscle regeneration in muscular dystrophy. *Hum. Mol. Genet.*, **18**, 2584–2598.
60. Li, H., Mittal, A., Paul, P.K., Kumar, M., Srivastava, D.S., Tyagi, S.C. and Kumar, A. (2009) Tumor necrosis factor-related weak inducer of apoptosis augments matrix metalloproteinase 9 (MMP-9) production in skeletal muscle through the activation of nuclear factor-κB-inducing kinase and p38 mitogen-activated protein kinase. *J. Biol. Chem.*, **284**, 4439–4450.
61. Acharyya, S., Villalta, S.A., Bakkar, N., Bupha-Intr, T., Janssen, P.M., Carathers, M., Li, Z.W., Beg, A.A., Ghosh, S., Sahenk, Z., Weinstein, M. *et al.* (2007) Interplay of IKK/NF-kappaB signaling in macrophages and myofibers promotes muscle degeneration in Duchenne muscular dystrophy. *J. Clin. Invest.*, **117**, 889–901.
62. Cai, D., Frantz, J.D., Tawa, N.E. Jr, Melendez, P.A., Oh, B.C., Lidov, H.G., Hasselgren, P.O., Frontera, W.R., Lee, J., Glass, D.J. and Shoelson, S.E. (2004) IKKbeta/NF-kappaB activation causes severe muscle wasting in mice. *Cell*, **119**, 285–298.
63. Yang, Q., Tang, Y., Imbrogno, K., Proto, J.D., Chen, A., Guo, F., Fu, F.H., Huard, J. and Wang, B. (2012) AAV-based shRNA silencing of NF-κB ameliorates muscle pathologies in mdx mice. *Gene Ther.*, 1–9.
64. Marshall, J.L., Holmberg, J., Chou, E., Ocampo, A.C., Oh, J., Lee, J., Peter, A.K., Martin, P.T. and Crosbie-Watson, R.H. (2012) Sarcospan-dependent Akt activation is required for utrophin expression and muscle regeneration. *J. Cell Biol.*, **197**, 1009–1027.
65. Welser, J.V., Rooney, J.E., Cohen, N.C., Gurpur, P.B., Singer, C.A., Evans, R.A., Haines, B.A. and Burkin, D.J. (2009) Myotendinous junction defects and reduced force transmission in mice that lack alpha7 integrin and utrophin. *Am. J. Pathol.*, **175**, 1545–1554.
66. Barton, E.R., Wang, B.J., Brisson, B.K. and Sweeney, H.L. (2010) Diaphragm displays early and progressive functional deficits in dysferlin-deficient mice. *Muscle Nerve*, **42**, 22–29.
67. Han, R., Kanagawa, M., Yoshida-Moriguchi, T., Rader, E.P., Ng, R.A., Michele, D.E., Muirhead, D.E., Kunz, S., Moore, S.A., Iannaccone, S.T. *et al.* (2009) Basal lamina strengthens cell membrane integrity via the laminin G domain-binding motif of alpha-dystroglycan. *Proc. Natl Acad. Sci. USA*, **106**, 12573–12579.
68. Charrin, S., le Naour, F., Silvie, O., Milhiet, P.E., Boucheix, C. and Rubinstein, E. (2009) Lateral organization of membrane proteins: tetraspanins spin their web. *Biochem. J.*, **420**, 133–154.
69. Stipp, C.S. (2010) Laminin-binding integrins and their tetraspanin partners as potential antimetastatic targets. *Expert Rev. Mol. Med.*, **12**, e3.
70. Yoshida, T., Pan, Y., Hanada, H., Iwata, Y. and Shigekawa, M. (1998) Bidirectional signaling between sarcoglycans and the integrin adhesion system in cultured L6 myocytes. *J. Biol. Chem.*, **273**, 1583–1590.
71. Crosbie, R.H., Lebakken, C.S., Holt, K.H., Venzke, D.P., Straub, V., Lee, J.C., Grady, R.M., Chamberlain, J.S., Sanes, J.R. and Campbell, K.P. (1999) Membrane targeting and stabilization of sarcospan is mediated by the sarcoglycan subcomplex. *J. Cell Biol.*, **145**, 153–165.
72. Allikian, M.J., Hack, A.A., Mewborn, S., Mayer, U. and McNally, E.M. (2004) Genetic compensation for sarcoglycan loss by integrin α7β1 in muscle. *J. Cell Sci.*, **117**, 3821–3830.
73. Hack, A.A., Cordier, L., Shoturma, D.I., Lam, M.Y., Sweeney, H.L. and McNally, E.M. (1999) Muscle degeneration without mechanical injury in sarcoglycan deficiency. *Cell Biol.*, **96**, 10723–10728.
74. Hack, A.A., Lam, M.J., Cordier, L., Shoturma, D.I., Ly, C.T., Hadhazy, M.A., Hadhazy, M.R., Sweeney, H.L. and McNally, E.M. (2000) Differential requirement for individual sarcoglycans and dystrophin in the assembly and function of the dystrophin-glycoprotein complex. *J. Cell Sci.*, **113**, 2535–2544.
75. Flintoff-Dye, N.L., Welser, J., Rooney, J., Scowen, P., Tamowski, S., Hatton, W. and Burkin, D.J. (2005) Role for the alpha7beta1 integrin in vascular development and integrity. *Dev. Dyn.*, **234**, 11–21.
76. Peter, A.K., Miller, G. and Crosbie, R.H. (2007) Disrupted mechanical stability of the dystrophin-glycoprotein complex causes severe muscular dystrophy in sarcospan transgenic mice. *J. Cell Sci.*, **120**, 996–1008.
77. Peter, A.K. and Crosbie, R.H. (2006) Hypertrophic response of Duchenne and limb-girdle muscular dystrophies is associated with activation of Akt pathway. *Exp. Cell Res.*, **312**, 2580–2591.
78. Bancroft, J.D. and Cook, H.C. (1985) Manual of histological techniques. In Chaplin, A.J. (ed.), *Methode de colorationelective du tissue conjonctif*. Churchill Livingstone, New York, Vol. 1905, pp. 1038–1040.
79. Jasmin, B.J., Alameddine, H., Lunde, J.A., Stetzkowski-Marden, F., Collin, H., Tinsley, J.M., Davies, K.E., Tomé, F.M., Parry, D.J. and Cartaud, J. (1995) Expression of utrophin and its mRNA in denervated *mdx* mouse muscle. *FEBS Lett.*, **374**, 393–398.
80. Barton, E.R., Morris, L., Kawana, M., Bish, L.T. and Toursel, T. (2005) Systemic administration of L-arginine benefits mdx skeletal muscle function. *Muscle Nerve*, **32**, 751–760.